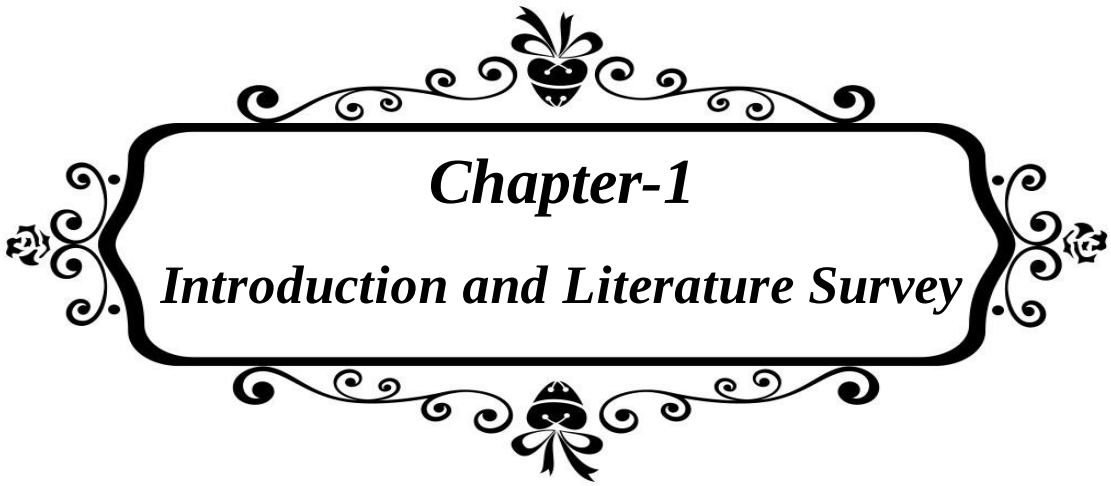

Chapter-1

Introduction and Literature Survey

1.1 Motivation and General Introduction

The energy requirement of the world is increasing year by year with the fast-growing economies and it is predicted that global energy demand will increase by 27% from 2018 to 2040. The projected trajectory of global energy demand is shown in the following chart prepared by International Energy Agency (IEA). After a dip in the curve in 2020 during covid pandemic, monotonous increase in the energy demand is foreseen.

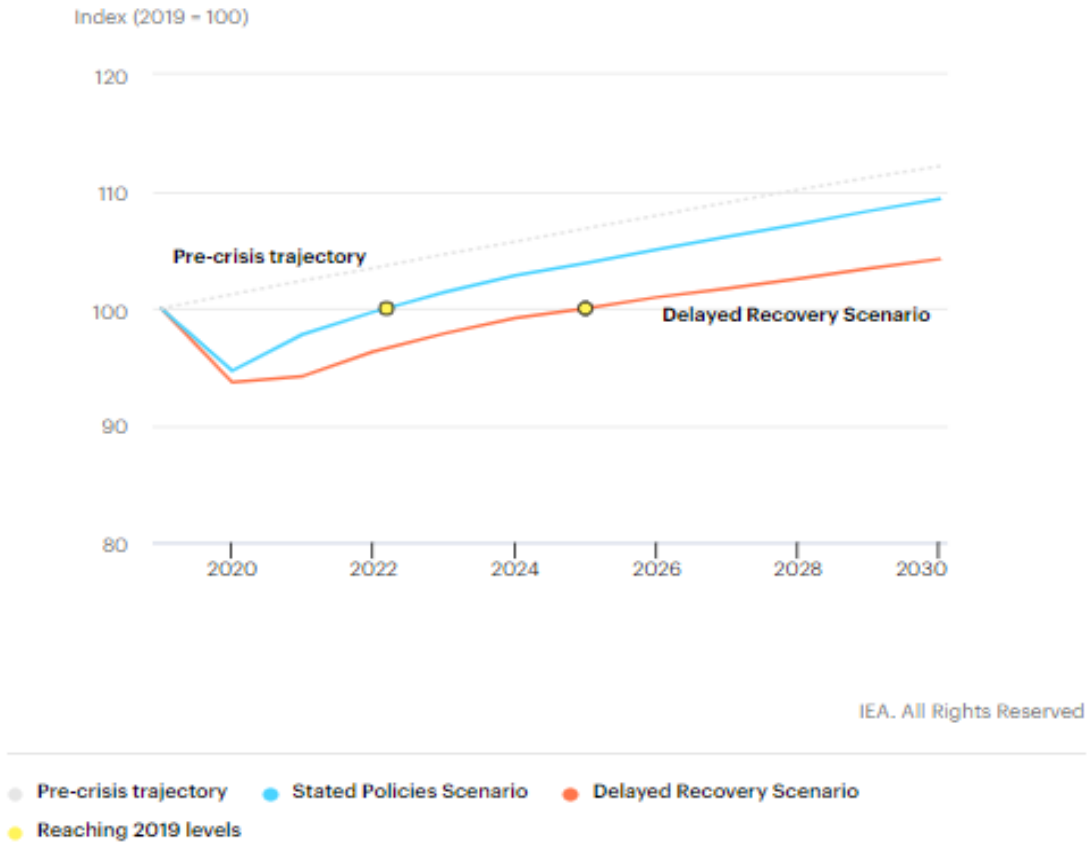

Figure 1.1: Global primary energy demand growth by scenario, 2019-2030 [1].

Currently, more than 75% of the Global energy demand is being fulfilled by non-renewable energy sources [2].Uncontrolled exploitation of limited fossil fuels such coal, oil, and gas resources will not only create challenging situations for our next as

generations but, increased emission of CO_2 due to its combustion, will cause climate change, respiratory diseases and increased wildfires. Dependencies on fossil fuels to fulfil the high demand of global energy have caused record 33.5 billion metric ton emission of CO_2 [3, 4]. Finding sufficient supply of alternate and renewable energy sources is the immediate and daunting challenge for the world energy society. The contribution of renewable energy sources has to be increased in the global energy consumption to prevent the depletion of underground fossil fuel reservoir and keep the environment clean. Currently, solar and wind energy contribute 64% of total energy from all type of different renewable energy resources. These two are major source of renewable energy. The share of solar energy contribution can be increased efficiently by enhancing the efficiency and by reducing the manufacture cost of the solar cell devices. Hence innovation and research development are essential to improve the efficiency and manufacture cost and thenceforth to make transition of energy dependency from fossil fuels to renewable energy sources.

Solar energy is a most abundant, sustainable, free and clean energy source which can be directly utilised through the photovoltaic (PV) effect. In coming decades, photovoltaic field appears to be most promising for renewable energy source to fulfil the global energy requirements. Energy of solar radiation falling on surface of earth every second in the form of photons is 12000 terawatts. If technological advancement can utilize only 0.2% of this energy with 10% efficiency, it will produce 24 terawatts, sufficient to fulfil the societal needs [5].

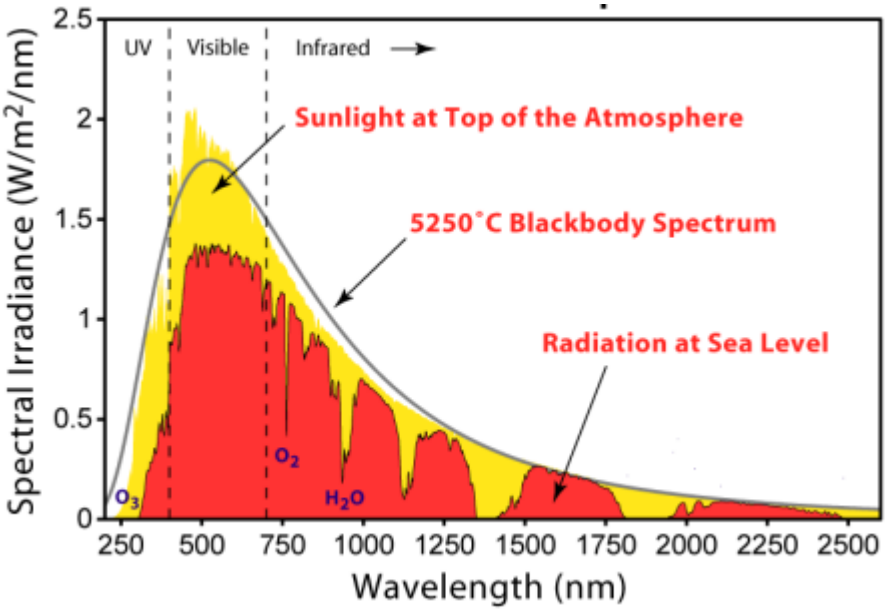

Figure 1.2: Intensity distribution of solar radiation against wavelength [6].

Since the first application of solar cells in the 1950s, fundamental and applied research and development, has efficaciously reduced their cost and they are most preferred power supply in some cases [7]. However, limitation of efficiency in conventional photovoltaic solar cells, unsustainable mining practices, toxic waste and CO_2 emission during photovoltaic panel production limit their contribution in the current energy supply market. Production of conventional photovoltaic solar cells mainly relies on crystalline silicon modules, which are much costly, being the major issue for economical commercialization of power harvesting from photovoltaic materials in comparison to non-renewable energy sources [8]. Emerging photovoltaic technologies such as organic cell, dye sensitized solar cells, perovskite solar cells, perovskite tandem solar cells etc. are being widely investigated for their low-cost manufacturing techniques and possibility of brisk increases of power conversion efficiency up to 24.2% within the last six years [9]. Chronicle evolution of various PV technology is shown in the Fig. 1.3. It can be seen that efficiency of perovskite solar

cells have been increasing rapidly. The efficiency evolution of C-Si thin film technology in 45 years, have been matched by perovskite solar cells only in 10 years.

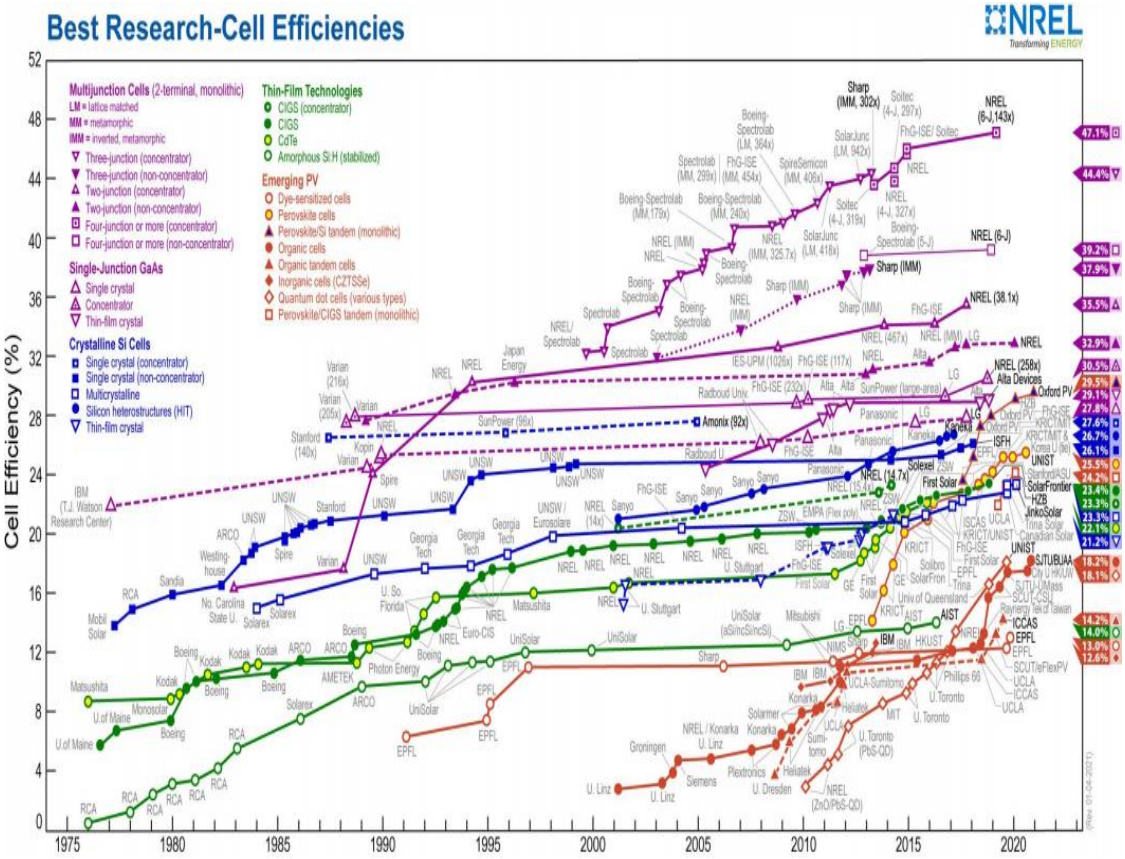

Figure 1.3: Time evolution of efficiencies of several photovoltaic solar cells [9].

Efficiency of conventional PV technologies depends on, charge carrier separation by the barrier field at p-n junctions, band gap of semiconductor material used, spectrum loss and recombination rate and maximum efficiency that can be achieved. Due to these factors, conventional p-n junction solar cells have theoretically limited efficiency of 31% to 41% depending on the concentration of solar light for Si based solar cells [10]. This maximum possible efficiency is known as Shockley-Queisser limit [11]. Thus, even half of the available solar energy cannot be utilized in ideal conditions by these conventional photovoltaic cells. However, there is a different PV mechanism in ferroelectric photovoltaic materials that is not constrained to inbuilt internal barrier fields [6]. Breaking of the inversion symmetry is the basis for this

mechanism. A polarization induced electric field separates the charge carriers which is present throughout the crystal. Because the entire crystal is uniformly effective for the photovoltaic response, it is also known as the "bulk photovoltaic effect" (BPVE). This effect in ferroelectric solar cells allows, above-band gap open-circuit voltages, surpass the Shockley-Queisser limit. This kind of solar cell uses ferroelectric materials which have facile synthesis process and are very cost-effective. Ferroelectric (FE) materials can show BPVE responses under unpolarized light throughout the crystal [12] and can also generate conventional PV carriers from the polarization-induced electric fields at grain boundaries, domain walls and interfaces of the electrodes [13]. Both, the BPVE and conventional PV effects in ferroelectric materials can make very high conversion efficiency feasible if a proper designing of ferroelectric material is done.

In spite of these attractive properties in FEPV materials, there are many challenges like high band gap, low conductivity, device fabrication process etc. stopping to achieve the desired efficiency, comparable to conventional p-n junction solar cells. A key challenge is to reduce the wide band gaps suitable to explore most part of the solar spectrum, without compromising the ferroelectricity. Because of highly insulating nature of perovskite oxides, commonly known ferroelectric materials like $BaTiO_3$, $PbTiO_3$, $KNbO_3$ etc. have very high band gap that falls in ultraviolet (UV) or even higher wavelength region [14-16]. The band gap engineering in these systems could potentially be approached through chemical substitution, quantum size effects, lattice mismatch in thin film formation or super lattice formation [17, 18]. The lowering strategies of band gap for bulk ferroelectric ceramics can provide a comprehensive idea of their PV performance in thin film or single crystal configurations. There are many attempts reported in literature to reduce the band gap by chemical alloying/substitution

[14, 15, 17-24]. These issues are addressed in detail in forthcoming pages of this chapter.

1.2 Photovoltaic solar cell

Solar energy incident on a material can be reflected, absorbed or transmitted through the material. When solar energy is absorbed by the material, the energy is transferred to electrons and creates excited electrons within the material, known as photoelectrons. Creation of these photoelectrons gives rise to many photo related phenomena such as photoconductivity (increase in conductivity due to photon absorption), Photo-Dember effect (creation of potential gradient due to photon absorption), photo dielectric effect (change of capacitance due to photon absorption) and photovoltaic effect (generation of free electrons due to photon absorption) [25]. The PV cell is composed of semiconductor material that absorbs light (photons) and generates charge carriers resulting as photocurrent. Photovoltaic effect is used in PV cells to generate electricity when light shines on it. There are various types of solar cells e.g., crystalline cells, single junction cells (p-n junction cells), multi junction cells, dye sensitized cells, perovskite cells etc. and amongst them, conventional p-n junction and ferroelectric photovoltaic solar cells are discussed in detail in subsequent sections.

1.2.1 Conventional p-n junction photovoltaic cells

The conventional PV cell is a simple p-n junction diode with heavily doped and thin n-side and lightly doped and thick p-side. A schematic diagram is shown in Fig. 1.4 showing the structure, band energy levels and I-V characteristic of p-n junction solar cells. It can be seen that a depletion region is formed at equilibrium at the interface when free electrons from the n- side diffuse across the junction filling the holes in the p-region, leaving immobile positive charges on n- side. Similarly immobile negative charges on p-side at the junction are generated when holes diffuse towards the n-side of

the material. The immobile charges in the depletion region induce an internal electric field which separates the e-h pairs generated in the depletion region after absorption of photons. Depletion region penetrates deep in p-region being it lightly doped and narrow in n-region being it heavily doped.

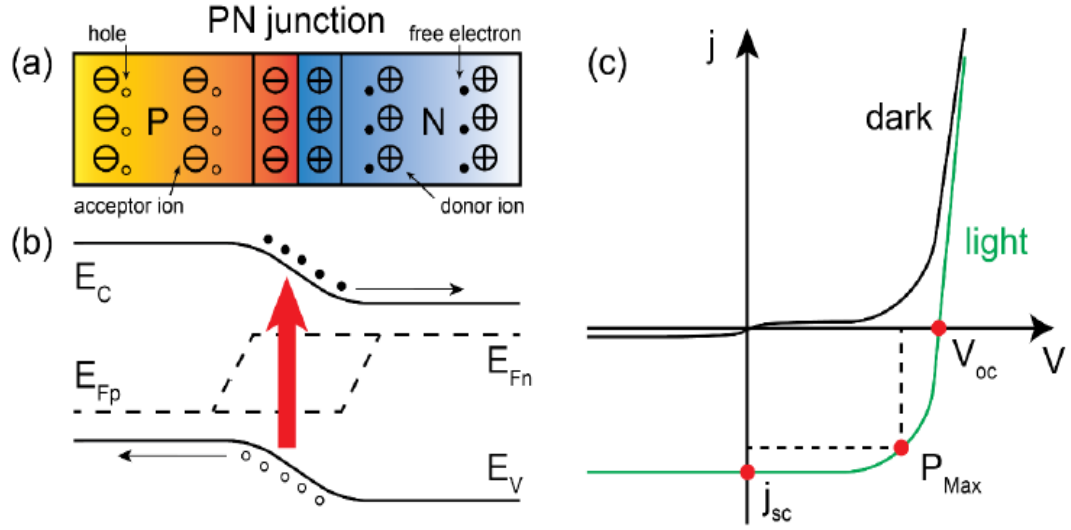

Figure 1.4: (a) A typical schematic junction diode. (b) Energy level diagram of a p-n junction (c) I-V characteristics junction based cell in the dark and under light [26].

Light is made incident on thinner n-side layer and it penetrates and reaches depletion region where photon is absorbed and e-h pair gets generated. These e-h pairs are then separated by the built in internal electric field in the manner that holes move towards the p-region and electrons move towards the n-region. If an external load (LED, fan, battery etc.) is connected to the solar cell, the excess electrons and excess holes deposited at the respective electrode recombine by travelling through the load and thus photocurrent is generated in the process. Electron and hole pair production also depends on the width of the depletion region, p-region and n-regions, as shown in Fig. 1.5. Radiation with longer wavelength penetrates more because absorption coefficient decreases for higher wavelengths. The shorter wavelengths could not penetrate much and are absorbed in the n region and longer wavelengths penetrates deeper and are

absorbed in the bulk of the p region. Photons with medium wavelengths can penetrate the n- region and reach depletion region where they are absorbed and create e-h pairs (EHPs). Most of the EHPs generated in these regions recombine but some EHPs contribute to the photo-current. Thus, different regions of the solar spectrum are absorbed at different parts (n-layer, junction layer and p-layer) of the device depending on the wavelength and the thickness of the n-layer, depletion layer and p-layer. Typical I-V characteristic of the solar cell is shown in Fig. 1.4 (c) with and without illumination of light. Under above–band gap illumination the characteristic curve obtained is almost similar to characteristic curve of p-n junction diode in dark with shift towards negative current axis and the shift depends upon intensity of illumination. More the shining, the curve will shift more negative side of current. The maximum current that can be extracted under an illumination is called short circuit current (J_{sc}) and the maximum voltage that can be obtained, is called open circuit voltage (V_{oc}) as shown in the figure 1.4 (c). The maximum power for realistic solar cell is expressed as $P_{max} = V_{oc} \times I_{sc} \times FF$ where FF is the Fill factor which tells about the quality of the solar cells, high FF value of a solar cell shows close to the ideal solar cell behaviour. For Si-based solar cells the value of FF is 80-85%. The charge transportation in the junction-based photovoltaic solar cells is often limited by weak diffusion across the depletion region. The V_{oc} is limited to the barrier potential at the junction, it cannot exceed barrier potential because separation of e-h pairs stops above it, which is generally 0.7-0.8V for Si. For these reasons, conventional photovoltaic energy harvesting based on crystalline silicon is less efficient and too expensive to prefer over fossil energy [27]. However, a p-n junction is not a mandatory requirement for the photovoltaic solar cells but other mechanisms such as ferroelectric polarization, gradient in a chemical potential or spin polarization can also be used for PV action in solar cells.

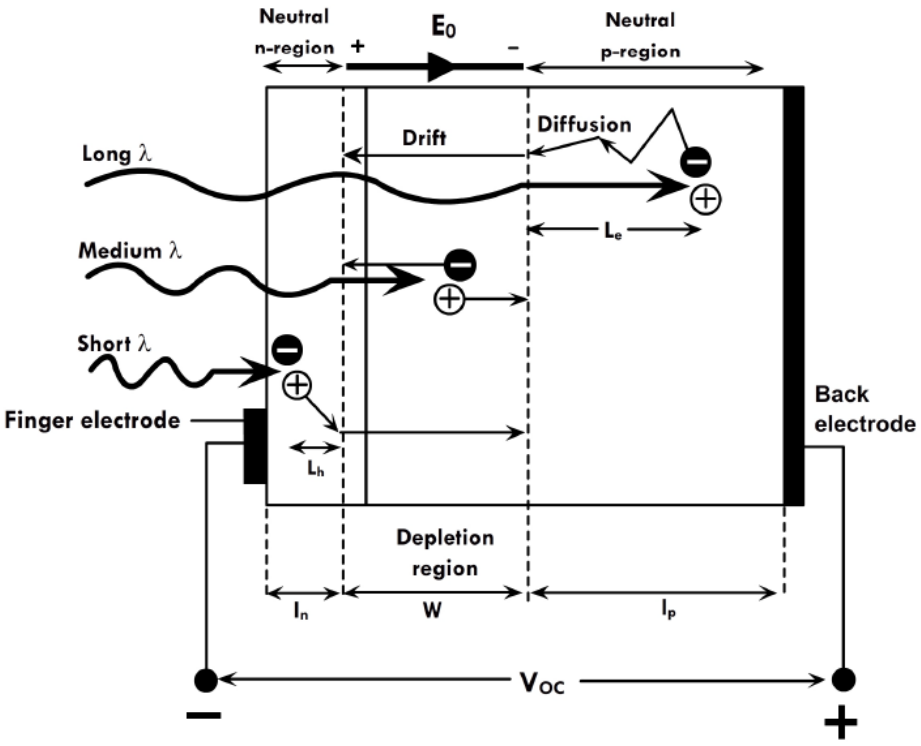

Figure 1.5: Interaction of radiation with p-n junction solar cell when illuminated through n-side surface [28].

1.2.2 Ferroelectric Photovoltaic Cells

Ferroelectric photovoltaic solar cells are the emerging photovoltaic cells based on ferroelectric materials. Ferroelectric materials can have permanent polarization induced electric field throughout the material even after removal of the external field. The mechanism of e-h pair separation in ferroelectric materials differs from p-n junction based photovoltaic effect. In ferroelectric materials, spontaneous polarization induces an internal electric field, which can provide efficient separation of photo-excited carriers, preventing the recombination rate to significantly small level [29]. There is absence of interface (p-n junction) like potential, but a polarization induced internal electric field is present which separates the e-h pair generated after absorption of photon. These photo generated electrons and holes are driven in opposite direction, contributing the photovoltaic output. Ferroelectric photovoltaic effect in ferroelectric materials is interconnected with the loss of inversion symmetry in the distribution of

polarization, space charges, defects and impurities [18, 30]. Polarization induced field is present throughout the crystal unlike to p-n junction solar cells where separation only takes place at depletion region and hence the separation of e-h pairs happens throughout the bulk region of the ferroelectric material popularly known as bulk photovoltaic effect (BPVE). This is fascinating phenomena with some unique features such as V_{oc} can be obtained more than the band gap (V_{oc} = 20V in $BiFeO_3$ band gap 2.2 eV-2.6 eV), [31-35] and photocurrent is proportional to the polarization magnitude [36, 37]. Fig. 1.6 (a) illustrates the structure and mechanism, while Fig. 1.6 (b) shows the I-V characteristic of a ferroelectric solar cell. It can be observed that under illumination, the photo current varies linearly with photovoltage at given polarization (P) unlike the I-V curve for p-n junction solar cell. It provides another feature that photo current and voltage can be switched by reversing the applied external field for polarization as shown in **Fig, 1.6 (b)** [37]. In ferroelectric materials, charge transportation is not limited to diffusion across a p-n junction and therefore V_{oc} is not restricted to potential barrier but it can increase with the increase in internal electrode distance in the polarization direction.

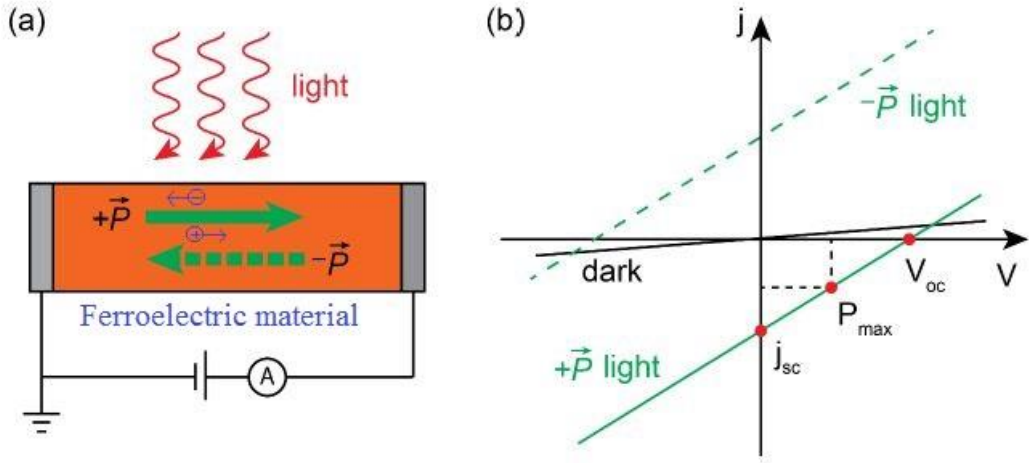

Figure 1.6: (a) Schematic diagram showing mechanism in FEPV solar cell (b) I-V characteristic in dark and in light of FEPV solar cell [37].

The light to electricity conversion efficiency in FEPV materials is of the order of 10^{-4} which is very low than the commercially available Si solar cell. Intrinsic low

conductivity of the ferroelectric domains is one of the major impediments in enhancing the efficiency. In reality, any effort to increase the conductivity of ferroelectric domains will lead to leaky domains and leakage in domains cannot withstand strong ferroelectric polarization because charge deposition across the domain walls reduces the band gap, resulting in a low open circuit voltage. Thus, low conductivity and wide band gap limits the efficiency of FEPV cells and proper innovation and research are required to combat these obstacles to make a competitive ferroelectric solar cell.

Presence of grain boundaries and the randomness of the grain orientations (and domain boundary orientation) make ferroelectric polycrystalline ceramics a complex material as compared to single crystals and epitaxial thin films. Hence, quantitative analysis of photovoltaic mechanism or contributions from the different PV mechanisms is challenging and no consistent reports are found on the working mechanisms of the observed PV effects in ceramic ferroelectric systems [35, 38-41]. However, shift current model and ballistic model are the most prominent mechanism explaining the high V_{oc} obtained in various ferroelectric materials. In ballistic mechanism, asymmetric distribution of their momenta causes excitation of non-thermalized (hot) carriers in a crystal. In shift model mechanism, the bulk photovoltaic effect is caused by carrier band–band transition and not by the carrier movement within the band. This model have quantum-mechanical nature [42, 43].

In photo-ferroelectric materials, ferroelectricity contains piezoelectricity and pyroelectricity simultaneously which responds to kinetic and thermal changes. This is a unique multi-functional property of photo-ferroelectrics which enables to harvest solar, kinetic and thermal energy within a single material. In such materials photovoltaic property can be used for harvesting energy whilst piezoelectric and pyro electric can be used for sensing applications.

1.2.3 Advantages of Ferroelectric Photovoltaic Cells

The ferroelectric photovoltaic cell has several advantages over conventional p-n junction based cells as listed below:

1. Polarization induced electric field separates the e-h pair, it works there without formation of p-n junction like complex structures.

2. There is absence of the potential barrier and extremely large open circuit voltage (V_{oc}), much higher than semiconductor band gap, can be obtained.

3. Open circuit voltage (V_{oc}) can be controlled by external electric field. It can be enhanced or reversed by increasing or reversing the polarization induced field.

4. Ferroelectric oxide materials are abundant, stable, cheap and have high absorption coefficient.

5. The large band gap and conductivity both can be simultaneously changed through chemical substitutions and thin film modulation in thin film ferroelectric photovoltaics.

6. Ferroelectric materials are also pyroelectric and piezoelectric simultaneously and these properties can be utilized for multifunctional devices.

7. The Magnetoelectric effect in composite/ multilayers of multiferroic materials can be exploited for magnetic field-controlled photovoltaics with added functionality.

8. It is also possible to utilise the spin polarization in multiferroic materials. Device miniaturization for optical micro-sensing and micro-actuation in micro-electro-mechanical systems can be the novel applications of these materials.

1.2.4 Limitations of Ferroelectric Photovoltaic effect

There are certain limitations also with the ferroelectric photovoltaics.

1. Most of ferroelectric materials have wide band gap which allow absorption of only UV region in solar spectrum. Band gap reduction of these materials is a challenge.

2. Intrinsically low conductivity of ferroelectric materials restricts in achieving high conversion efficiency.

3. Non-uniform internal polarization (P_s) throughout a ferroelectric gives rise to depolarizing field.

4. Whenever one tries to reduce the band gap of ferroelectric materials, the leakage current increases, that degrades its ferroelectric properties.

Recent discoveries also have revealed that ferroelectric materials can be very attractive for highly efficient photovoltaic applications. Presence of spontaneous polarization in ferroelectric materials, instead of the junction barrier field in conventional photovoltaic materials, enables the required separation of photo-excited carriers, and the photo voltage higher than the band gap. This is a crucial factor for enhancing the efficiency greater than traditional p-n junction based solar cells [31, 44]. Efficient and controllable carrier separation facilitated by polarization electric field, with peculiar properties make them very promising for low-cost high efficiency solar cells [22, 29, 45]. Tuning the band gap to usable region of solar spectrum in typical ferroelectrics without reducing the polarization at usual condition will provide an ideal photovoltaic material for solar energy harvesting. In order to achieve low fabrication cost, stable and more efficient solar cells, there is large surge of research in ferroelectric photovoltaic materials [46, 47].

1.3 Materials used for FEPV solar energy harvesting

1.3.1 Perovskite materials

Most interesting and important ferroelectrics belong to ABO_3 perovskite oxides family, thanks to strong polarizability, good ferroelectric response and occurrence of multiple crystallographic ferroelectric phases presenting morphotropic phase boundaries. Common important perovskite ferroelectric materials investigated in detail

for various applications are $BaTiO_3$,[48-50]. (1-x)$KNbO_3$-x$Ba(Ni_{1/2}Nb_{1/2})O_{3-\delta}$, $BiFeO_3$[51], $KNbO_3$[29, 52], $Pb(Zr,Ti)O_3$[53], $PbTiO_3$ [54, 55] etc. and solid solutions based on them. However, wide band gap (> 3 eV) associated with these materials have restricted to utilise them in usable solar spectrum leading to poor conversion efficiency. The wide band gap is mainly due to 'high electronegativity difference' between oxygen and transition metals, specifically at B-site. The transition metal cations play a crucial role in determining the band gap of perovskite oxides [56].

Perovskite structure with general formula ABO_3, where A and B sites are filled by cations with cation valence equal to the anion valence, is one of the most versatile structures which dominates the world of useful ceramics. The perovskites have shown the multifunctional flexible structure and the properties. Perovskite is the only structure which can produce wide array of phases having different properties by skilled chemical substitution at A- and B-site cations. Perovskites exhibit very flexible crystal structure; they can accommodate more than 90% of the metallic elements present in the periodic table. Ideally perovskites adopt cubic structure with ABO_3 like chemical formula where A and B are metal cations, cation-A at the corners of cube, cation-B at the centre of the cube and O-anion at the face centres of the cube as shown in Fig. 1.6. It is notable that when bonding is entirely ionic in perovskites, it is always centrosymmetric (cubic) and therefore not ferroelectric. Because, in case of ionic bonding, the coulombic repulsion of electron clouds on adjacent ions is minimized in centrosymmetric structures [57]. It is evident that O-ions at the faces of cube forms an octahedron with B-cations at the centre and any tilt/rotation or distortion of this octahedron give rise to deviation from ideal cubic structure resulting in different structure of lower symmetries (tetragonal, rhombohedra, orthorhombic, monoclinic, etc.). Goldschmidt predicted a tolerance factor

criteria that tells the deviation from cubic structure and predicts the stable crystal structure of perovskites [58], defined by

$$t = \frac{r_A + r_o}{\sqrt{2} \times (r_B + r_o)} \quad (1.1)$$

where r_A, r_B and r_o represent the radii of A-cation with 12-fold oxygen coordination, B-cation with 6-fold oxygen coordination and O-anion respectively. The value of 't' will suggest the compatibility of the cations with crystal structure. If the value of t >1 (A-cation too big or B-cation too small), tetragonal or hexagonal crystal structures is observed e.g. $BaTiO_3$, $BaNiO_3$ etc. For t < 1 and t = 0.9 to 1 (A and B have ideal size) cubic crystal structure is adopted for example $SrTiO_3$. For t < 1 and t = 0.71 to 0.90 (A-cation is too small to fit into B-inter sites), the crystal is stabilized in orthorhombic or rhombohedral structure e.g. $GdFeO_3$ and $CaTiO_3$. For t < 0.71 (A and B have similar radii) different structures like trigonal are observed e.g. $FeTiO_3$.

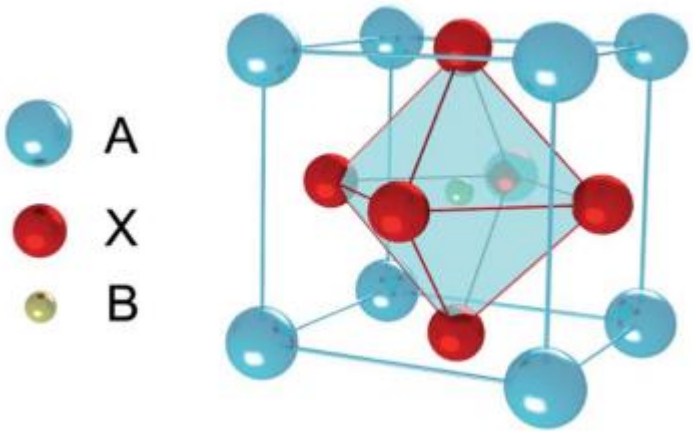

Figure 1.7: Typical crystal structure of perovskite (ABO_3) type materials [59].

Proper modifications of A-O and B-O bonds characteristics, may shift band gap to visible region and make them suitable to utilise in the complete solar spectrum for efficient energy harvesting. But, whenever, B-site ion substitution is performed in order to reduce the band gap, it also leads to the depreciation of dielectric and ferroelectric

properties specially polarization [60]. It is highly desirable to search for a material which can exhibit large polarization and low band gap simultaneously.

Another kind of perovskites are organometallic halide perovskite ($CH_3NH_3PbX_3$) where X = I, Br and Cl at the site of oxygen, Pb is at the B site and $CH_3NH_3^+$ at the A site. These were selected as one of the biggest breakthrough material in 2013 [61]. In organometallic perovskites, a perovskite solar cell with a PCE of 9.7% was reported in 2012, then a little higher and certified PCE of 17.9% was shown in 2014. Power Conversion Efficiency of 19.3% was also reported in the same year (2014). However, these organometallic perovskites suffer from the stability issues restricting their large-scale commercial applications.

1.4 Factors affecting the cell conversion efficiency

Conversion of electromagnetic radiation into electrical energy by photovoltaic effect is not a straightforward phenomenon and therefore the conversion efficiency depends upon numerous direct and indirect factors. Some of them are listed below.

1.4.1 Mechanism of the energy conversion in the solar cell

The energy conversion mechanism involved in conventional solar cell is based on charge carrier separation by the barrier field at p-n junctions and it has maximum efficiency limit, given as Shockley-Queisser limit (32%). However, mechanism is completely different in ferro-photovoltaic solar cells, where polarization induced electric field separates the charge carriers. Thus, with the progression of research, the emerging photovoltaic cells can achieve much better efficiency than junction based solar cells. Apart from the energy conversion mechanism, characteristic physical properties of the materials like purity, mobility, band gap and conductivity also crucially define the conversion efficiency of photons into electricity.

1.4.2 Wavelength of light

A solar cell cannot respond to the entire spectrum of sunlight, but, only specific range of wavelengths, is able to excite the electrons. When light strikes a material, some photons are reflected, some are transmitted and some are absorbed. Only a portion of this absorbed wavelength has enough energy (greater than the band gap energy) to separate the electrons from their bond, resulting into e-h pair, and rest of the photons are only able to generate heat.

1.4.3 Band gap

Band gap energy is the energy required to excite an electron from valence band to conduction band, eventually generating a hole in the valence band. Photons having smaller energy than the band gap of material are not absorbed and photons with higher energy than the band gap are do absorbed but the excess energy are wasted in re-emitting of heat and light. So major portion of solar spectrum light energy is wasted due to this band gap mismatch. Materials with variable band gap can enhance the cell efficiency remarkably. The band gap in classical semiconductors varies with composition in non-linear manner. Therefore, it is very important to understand the compositional effects and other fundamental parameters that affect the band gap.

1. Orbital Overlap

The interaction of order of more than 10^{23} atomic orbitals in a solid give rise to formation of energy bands. As the orbitals consist of electron wave function overlap, their interaction broadens the energy band due to Pauli's exclusion principle. The overlapping of orbitals and formation of band gap is shown schematically in Fig. 1.8. The band gap depends on type of orbitals forming the conduction and valence band, energy difference between the overlapping orbitals and the degree of interaction.

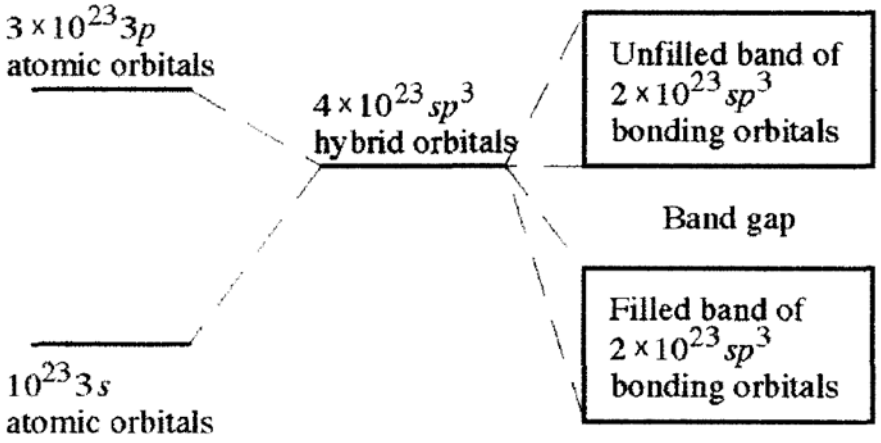

Figure 1.8: Schematic diagram showing the overlapping of orbitals in Si- crystal to form the band gap [62].

The band gap in perovskites (ABO_3) involves essentially the energy difference between oxygen 2p-orbitals and 3d-orbitals of transition metal cation at B site. Cations occupying the B-site and their suitable substitution will modify the 3d-orbitals and thus the conduction band. As much low is the energy level of 3d-orbital of cation at B site, that much low will be the band gap as presented schematically in Fig. 1.9.

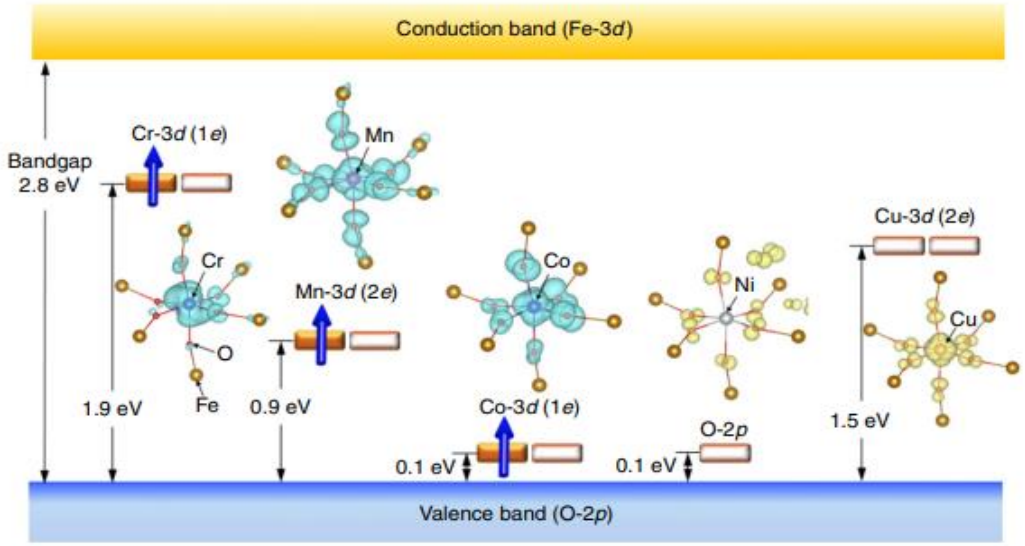

Figure 1.9: Variation of band gap in $BiFeO_3$ (ABO_3) perovskite with transition metal doping [30].

Degree of interaction depends on the distance between the atoms and spatial delocalization of the orbitals. Interaction of the orbitals increases with the increase of

the size of atoms. Increased interaction makes the energy bands wider and hence the gap between the bands reduces. For Example-the size of carbon, is much smaller than Silicon and Silicon is smaller than germanium. In carbon the interaction happens between n = 2 electrons, while in Si between n = 3 and in Ge between n = 4 electrons and thus band gaps observed for C (5.33 eV), Si (1.12 eV) and Ge (0.74 eV) respectively are in decreasing order opposite to the increasing order of size of the atoms [62].

2. Electronegativity

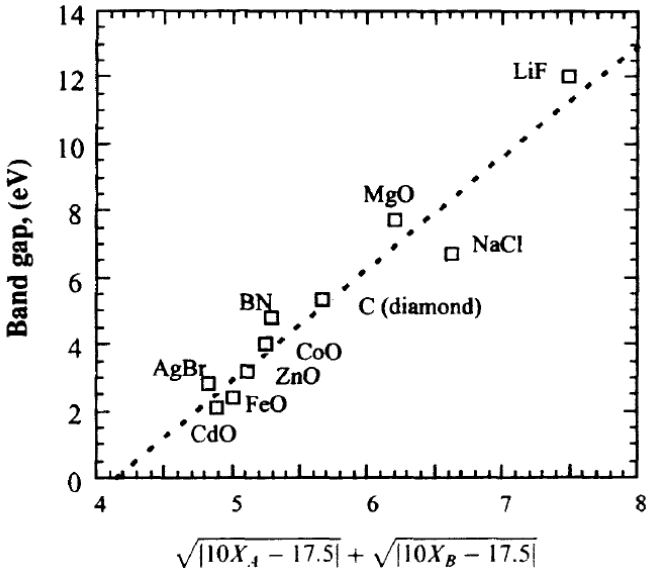

Figure 1.10: Electronegativity and band gap empirical correlation (X_A and X_B are the electronegativity's of the constituent atoms) [62].

According to tight bonding theory, as the electronegativity increases, the energy band become narrower and the region of forbidden energy gap widens resulting into the increased band gap. According to this theory, an empirical correlation can be expressed for the band gap (E_g) as:

$$E_g(eV) = 15 + 3.75\sqrt{|10X_A - 17.5|} + \sqrt{|10X_B - 17.5|} \qquad (1.2)$$

It is illustrated by Fig. 1.10, where X_A and X_B are the electronegativities of the atoms making the solid. Thus, for lower band gap, the individual electronegativity of the constituent atoms and electronegativity difference between the constituent atoms should be lower.

3. Crystal structure of the material

The splitting of energy levels of 3d-state (t_{2g} and e_g) of a transition metal cation in octahedral site is different than tetrahedral site. The splitting of t_{2g} and e_g is more in octahedral site than in tetrahedral site as shown in Fig. 1.11. Thus, a material with same molecular formula but different crystal structure may have different band gap. In typical ferroelectric materials (e.g. $BaTiO_3$), conduction band maximum (CBM) is composed of Ti-t_{2g} (d_{xy}, d_{yz} and d_{xz}) states and valence band consists of O-2p states. The change in contribution of the individual orbital of transition metal forming the conduction band minima makes the impactful difference. The contributions of d_{yz} and d_{xz} of transition metal's orbitals band are substantial enough in forming the conduction band to generate a large bulk photo voltaic effect [35].

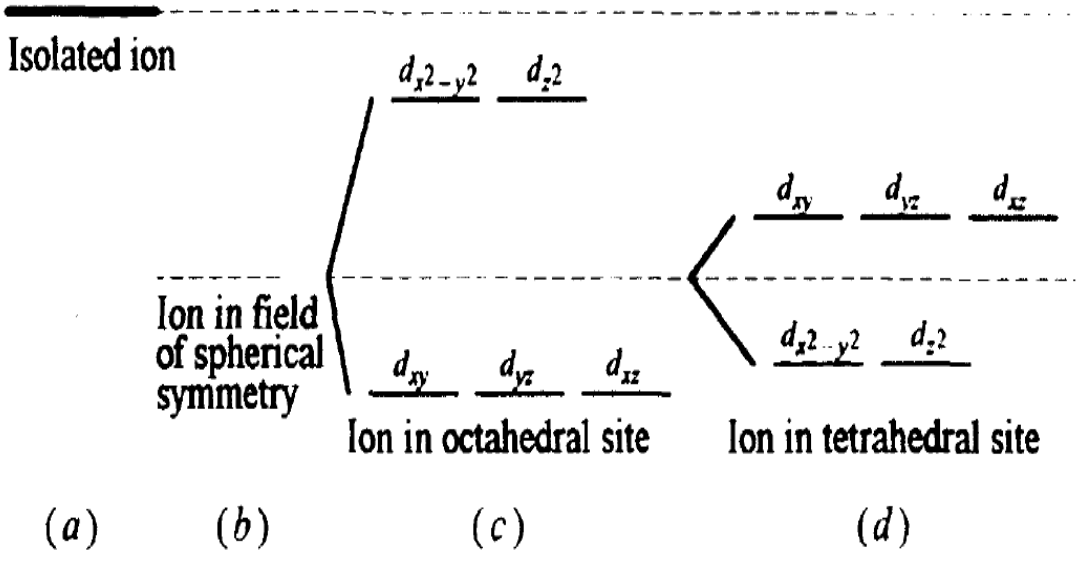

Figure 1.11: Energy of d-orbital of transition metal cation (a) in free or isolated ion (b) in field of spherical symmetry (c) with ion in octahedral site (d) with ion in tetrahedral site [62].

In perovskites, the effects of the octahedral tilt and lattice volume follow a systematic trend on the band gap. The variation of band gap of the doped material (solid solution) does not follow a single bowing behaviour but follows Vegard's law. Band gap of a general perovskite solid solution $A_{(1-x)}B_xC_{1-y}D_yO_3$ can be shown by the following equation.

$$\boldsymbol{E_g}\left(A_{(1-X)}B_xC_{(1-y)}D_yO_3\right) = (1-x)\boldsymbol{E_g}(ACO_3) + x\boldsymbol{E_g}(BCO_3) + (1-y)\boldsymbol{E_g}(ACO_3) + y\boldsymbol{E_g}(ADO_3) + \boldsymbol{E_g}(excess) \quad (1.3)$$

where $\boldsymbol{E_g}(ACO_3)$, $\boldsymbol{E_g}(BCO_3)$and $\boldsymbol{E_g}(ADO_3)$ denote the band gap of each perovskite end member. $\boldsymbol{E_g}(excess)$ denotes the excess band gap energy of mixing given by the following formula-

$$\boldsymbol{E_g}(excess) = W_{ACO_3}x^2(1-x) + W_{BCO_3}x(1-x)^2 + W_{ACO_3}(1-y)y^2 + W_{ADO_3}y(1-y)^2 \quad (1.4)$$

Where W_{ACO_3}, W_{BCO_3}, W_{ADO_3} are weighting parameters, proportional to the band gap energy of the respective end members. $\boldsymbol{E_g}(excess)$ is dependent on the concentration of each component. [62]

1.4.4 Electrical Conductivity

Apart from wide band gap, the main restricting factor for photovoltaics in ferroelectric materials is the poor conductivity. Typical ferroelectric like $Pb(Zr,Ti)O_3$ and $BaTiO_3$ based materials show very low conductivity of the order of 10^{-9} S/m at room temperature. The inherent resistance of the materials offered to the charge carriers from flowing plays a crucial role in reducing the efficiency. As much low resistivity is shown by the material, so much easily electrons and holes will be able to reach the respective electrodes. In bulk ceramics, conductivity is enhanced by formation of oxygen vacancies for the sake of charge neutrality. Doping of hetero-valent cations at A

and B-sites, creates a deficit of the positive charge which is balanced by reducing the negative charge, leading to removal of oxygen anions, and hence, charged oxygen vacancies (V_O) are formed. This treatment is described by the Kröger–Vink approach in ionic crystals [14]. Band gap reduction improves the conductivity of the material also along with the absorption of solar radiation.

1.4.5 Reflection

When light falls on the solar cell active material, a part of total incident light enters and rest is reflected back. These reflected back photons cannot excite the electron and thus cannot create e-h pair. Usually, untreated material surface reflects 20% to 30 % of the incident light which is needed to be addressed to increase the efficiency. Various antireflection surface technologies are applied to optimize the total absorption and better results are observed for multiple antireflective layers.

1.4.6 Temperature

Solar cell materials work optimally at low temperature, the efficiency decreases as the operating temperature rises. Perovskite halide and Si, Ge based solar cells are temperature sensitive materials. Thermal instability is one of the main challenging issues in these materials. Ferroelectric photovoltaic materials are thermally most stable materials for photovoltaic application.

1.5 Ferroelectricity and its Types

Ferroelectric materials possess spontaneous electrical polarization which can be reversed by reversing the external electric field. In the absence of an electric field, spontaneous polarization has stable orientation, which can be reoriented by changing the strength and direction of external electric field. In addition, ferroelectric materials have wide variety of physical and electronic properties useful in various applications like non-volatile memory, field effect transistors, tunable capacitors, solar cells etc.

Rochelle salt ($NaKC_2H_4O_6.4H_2O$) was the material in which ferroelectricity were first discovered by J. Valasek in 1920 [10]. In ferroelectric materials, energy minimization condition requires formation of several regions with electric dipoles having same alignment in particular region, the resulting state are known as domain structure. Presence of domain structure in ferroelectric materials is responsible for hysteresis loop behavior of these materials. All the ferroelectrics undergoes a phase transition from a higher symmetry (paraelectric state) to lower symmetry (ferroic state) when they are cooled below a particular critical temperature, knows as Curie temperature (T_c) of the material. For example, paraelectric (cubic) $PbTiO_3$ changes to ferroelectric (tetragonal) below T_C~753K [63]. There are multiple mechanisms for originating ferroelectricity in materials: (i) Ferroelectricity due to d^0 orbitals, (ii) Ferroelectricity due to non-bonding e-lone pairs, (iii) Ferroelectricity due to charge ordering of different cations, (iv) Geometric Ferroelectricity. The origin of ferroelectricity due to these mechanisms is briefly discussed below.

1.5.1 Ferroelectricity due to d^0 orbitals

Ferroelectric stability is governed by a delicate balance between short-range repulsions between electron clouds and additional bonding considerations between the atoms. Short-range columbic repulsion between electron clouds favours the non-ferroelectric centrosymmetric structure whereas partial covalent character of bonding induces the stabilization of ferroelectric phase. The microscopic origin of ferroelectricity in many ABO_3 perovskites is due to ligand field hybridization, which requires metal ions with empty d-orbital, such as Ti^{4+}, Nb^{5+}, Ta^{5+}, W^{6+} etc. The empty d- orbital in metal cation needs to hybridize with O-2p orbital and form covalent bonding character with particular orientation in bonds, which breaks the centre of symmetry in the structure to develop polarization. In contrast, the partially filled d-orbitals are responsible for the

magnetism in many magnetic materials. As shown schematically in Fig. 1.12, in mixed solid solution of empty and partially filled d-orbitals, magnetism is caused by partially filled d^n ions (red arrows) whereas ferroelectricity is caused by d^0 ions (green). Partial covalent character, because of hybridization of empty d-orbitals and O-2p orbitals, leads to the shift of cation from the center of O_6 octahedra (yellow plaquettes) causing polarization [64, 65].

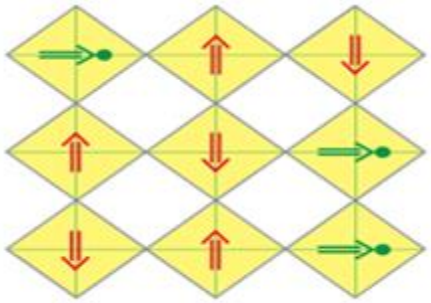

Figure 1.12: Off centering of d^0 ion (green circles) and magnetic moment of d^n ions (red arrows) in a mixed solid solution [64].

1.5.2 Ferroelectricity due to lone pairs

In some materials like $BiFeO_3$ and $PbTiO_3$, the major ferroelectric distortion is caused due to the presence of electron lone pairs lying in oxygen octahedral cage. The Pb^{2+} and Bi^{+3} ions have a lone pair of $6s^2$ outer shell electrons, which are not involved in chemical bonding and are called dangling electrons.

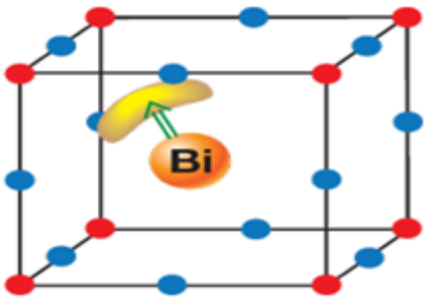

Figure 1.13: Illustration of distortion due to lone pair of Bi [64].

These lone pair electrons break the local inversion symmetry. Moreover, these electrons hybridize with p-orbital of oxygen resulting in structural distortion shown by green arrow [64].

1.5.3 Ferroelectricity due to charge ordering

When a parent material is doped with multiple valences and the ions are distributed in ordered way then ordering of charge happens. Charge ordering is seen primarily in transition metal compounds and with ions containing mixed valences. In this ordering the bond lengths change, leading to asymmetric distribution of charge resulting in stable polarization. For example, ferroelectricity in $LuFe_2O_4$ (T_c = 330K) is reported to be originating by this mechanism [66].

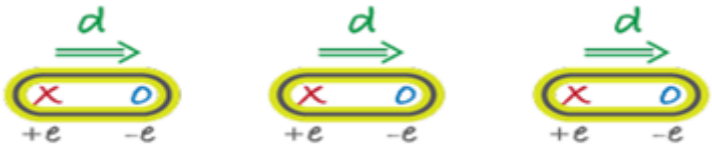

Figure 1.14: Schematic diagram for charge-ordering in ferroelectric materials [64].

1.5.4 Geometrical Ferroelectricity

Ferroelectric states, where polarization induces due to the structural distortion falls under this category. For example, ferroelectricity in $YMnO_3$ is caused by tilting a rigid MnO_5 block unit. Because of this tilting, Y and oxygen ions come closer to each other and form a dipole (green arrows), producing a polarization in a particular direction as shown in Fig.1.15 [57].

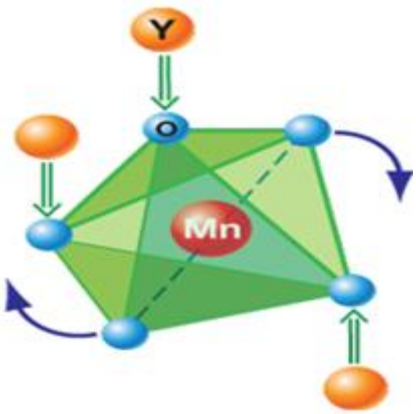

Figure 1.15: Schematic diagram for geometrically frustrated distortion [64].

1.5.5 Magnetically Driven Ferroelectrics

In these materials, ferroelectricity is induced by the external magnetic field. The material exhibits strong magneto-electric coupling due to which ferroelectricity is strongly influenced by an external magnetic field.

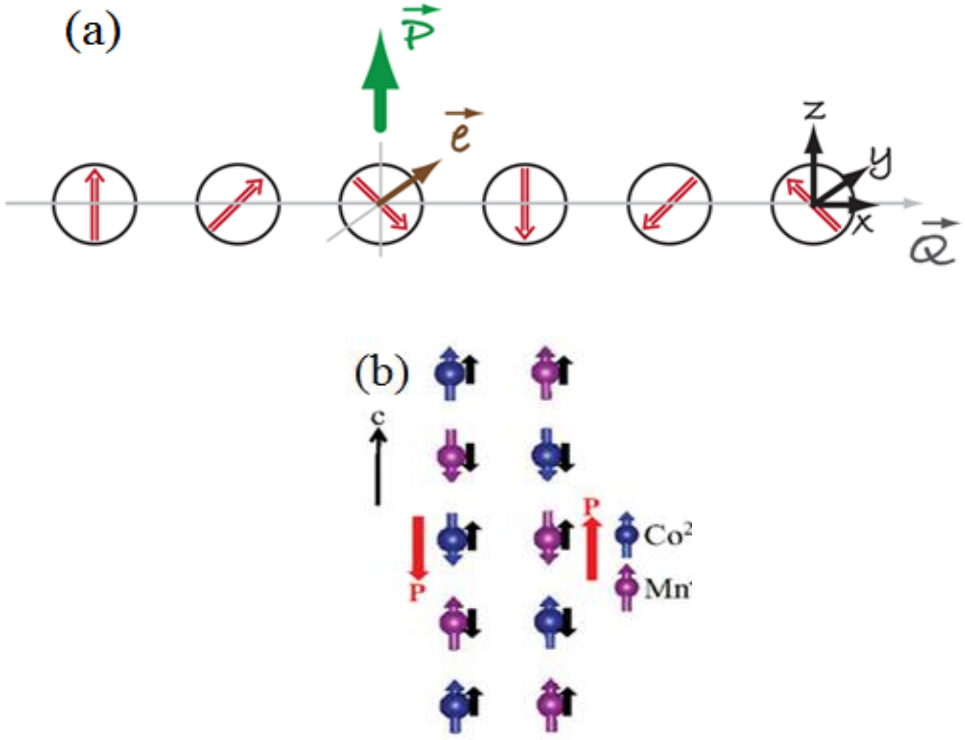

Figure 1.16: (a) The cycloidal spiral spin ordering with the wave vector Q = Q_x and spins rotating in the (x-z) plane. (b) Co/Mn collinear chain with two states of spin ordering in Ca_3CoMnO_6 [67].

Typically, these materials have centrosymmetric structure and show weak polarization. There are observed two type of spin ordering, spiral and collinear. In the spiral structure, ferroelectricity is induced in magnetic phases with spiral magnetic structure breaking the inversion symmetry e.g. $RMnO_3$ (R=rare-earth elements), whereas in collinear magnetic structure, ferroelectricity originates from magneto-striction e.g. Ca_3CoMnO_6. Fig. 1.16(a) shows the schematic diagram of cycloidal spiral spin ordering resulting in non-zero polarization. In Fig. 1.16(b), two states of spin ordering Co and Mn collinearly can be seen. The magneto-striction in these collinear ordered spins result in electric polarization.

1.6 Strategies to make efficient ferroelectric photovoltaic materials

As discussed in earlier sections, various approaches like domain wall engineering, thin film size reduction, chemical substitutions etc. are being adopted to overcome the poor absorption and low photocurrent in FE materials and to bring down the wide band gap near to ideal value. A suitable material for photovoltaic applications must have (i) band gap below 2.0 eV to cover more than 50% region of the solar spectrum, (ii) significant light absorption coefficient of 10^4–10^5 cm^{-1} and (iii) carrier concentrations in the range of 10^{15}–10^{17} cm^{-3}. Both, the absorption coefficient as well as carrier concentrations, can also be improved during the process of lowering the band gap [68, 69]. The first step to increase efficiency of photo-conversion is generation and proper dissociation of exciton (separation of e-h pair) and then the next is conduction of dissociated electrons and holes to their respective electrodes. Generation of e-h pairs on photon illumination is directly related to its optical band gap, lower the band gap of material, higher the absorption of photons. The most challenging issue in ferroelectric photovoltaic materials is the wide band gap of material. Typical ferroelectric materials like $PbTiO_3$, $BaTiO_3$ and $KNbO_3$ have band gap more than 3.0 eV which can only absorb ultra violet light constituting only 3.5% of solar spectrum and any attempt to reduce band gap in such materials deteriorates ferroelectricity [60]. Therefore, it is

extremely essential to decrease the band gap for higher absorption and significant photocurrent. Maximum conversion efficiency for air mass (AM) 1.5G radiation is observed at 1.34 eV and the permissible variable range of band gap is 0.67 eV for which the efficiency can be achieved 90% of the Shockely Quiesser limit [10, 68]. Therefore, materials with variable or multi band gap may provide a range of band gap energy and thus can enhance the efficiency significantly. In this context, multiferroic materials which can show ferroelectricity in absence of d^0 ness of B-site cation deserve considerable attention, for designing a low band gap ferroelectric photovoltaic materials [70].

Many strategies have been adopted to modify the band gap of ferroelectric materials. In this context, doping of transition metal cations at A and B-sites of the ABO_3 perovskite structure have shown great potential. R. Inoue et. al. have reported two Mn-d defect energy states in the conduction band, formed at 1.8 eV and 1.2 eV with respect to valence band maximum in Mn-doped single crystal $BaTiO_3$. The Mn-doping not only reduced the band gap but also improved the photocurrent from $J_{sc} \sim 36$ pA/cm^2 to 285 pA/cm^2, when doped with 0.25% Mn under the $h\nu < 2$ eV light irradiation. The excitation of electron from O-2p valence band to the Mn- e_g defect level is followed by hole injection, thus increasing the photocurrent [71]. Recent theoretical studies have suggested that doping of d^8 M^{2+} (M = Ni, Pd, Pt, and Ce) transition metal cations in TiO_6 network stabilized oxygen-vacancies, that reduces E_g less than 2.0 eV [72, 73]. Another study suggested that in completely filled or empty d-states and highly tetragonal structure, the band gap can be lowered by B-site ordering with layered structure or by tilting the oxygen tetrahedron [74]. However, these structures are predicted theoretically and have to be realized yet experimentally [23, 75, 76]. Zhang et al. have reported that reducing oxygen coordination number is another strategy to lower

the band gap in ferroelectric materials. Indeed, tetrahedral compounds which have smaller coordination number as compared to octahedral compounds, are intrinsically polar and inverted t_{2g}/e_g orbitals in them lead to a smaller band gap [68]. Zhang et al. have prepared a new multiferroic $KBiFe_2O_5$ with $E_g \sim 1.6$ eV and $J_{sc} \sim 15$ $\mu A/cm^2$ and $V_{oc} \sim 9.1V$. Nechache et. al. have applied cationic ordering strategy to prepare Bi_2FeCrO_6 and achieved the band gap $E_g \sim 1.4$ eV, $J_{sc} \sim 20.6$ mA/cm^2 with $\eta = 8.1\%$. An innovative strategy has been reported by H. Matsuo et. al. that is 'gap-state' engineering. In this approach defect states are created within the band gap and half of these defect states are filled with electrons and other half is kept empty [30]. Under the illumination of even below band gap energy, empty states receive electrons from the valence band and fill the defect state and the filled defect states supply electron to conduction band. Thus, generating electron-hole pairs even below the band gap energy**.** **Fig 1.9** shows the schematic diagram of gap states band structure co–produced by Cr, Mn and Co transition element doping in $BiFeO_3$. The theoretical as well as experimental findings reveal that gap states improve both the photocurrent and photovoltage [30]. For example, Mn-doped $BiFeO_3$ shows one order better photocurrent $J_y \sim -15\mu A/cm^2$ than that of film ($\sim J_y \sim 1.3\mu A/cm^2$).

1.7 An overview of ferroelectric photovoltaic Materials

Various research groups all over the world are carrying out continued efforts in the field of oxide based photovoltaic cells to enhance the efficiency and find out better alternative of silicon solar cells. Ferroelectric oxide photovoltaics, owing to their low-cost fabrication method and unmatched stability have been investigated rigorously over the past ten years. However, in spite of large number of known ferroelectric oxide materials, only few are well studied for photovoltaic effect. Henceforth, we will review

and discuss the photovoltaic phenomenon reported in typical ferroelectrics $PbTiO_3$, $BiFeO_3$, $BiMnO_3$ and $BaTiO_3$ based materials for photovoltaic applications.

1.7.1 Lead Titanate ($PbTiO_3$) and its solid solutions

The $PbTiO_3$ and its solid solutions are extensively investigated materials for photovoltaic applications. $PbTiO_3$ draw attention due to very high room temperature spontaneous polarization (Ps = 59$\mu C/cm^2$). For the first time M. Fridkin et. al. observed photocurrent in the direction of spontaneous polarization in the single crystals $PbTiO_3$. They also observed change in photocurrent with temperature and light intensity [77]. The ferroelectricity in $PbTiO_3$ based materials is correlated to strain in the lattice in such a way that larger crystallographic distortion leads to higher polarization [78]. Thus, tetragonality of $PbTiO_3$ is to be retained or enhanced while modifying for lowering the band gap to avoid supressing of polarization.

Many existing reports in literature suggests that, B-site (Ti) substitution in the $PbTiO_3$ with suitable transition-metal cations can make the bonding with oxygen more covalent or less ionic and reduce the band gap [54]. The cationic displacement at the B-site is also responsible for driving ferroelectricity in these ferroelectrics [56]. Conduction band and valence band involves 3d-orbital at B-site cations and 2p-orbital of the oxygen respectively. It was predicted theoretically that Ni, Pd and Pt doped $PbTiO_3$ show a reduced band gap without supressing the polarization as illustrated in **Fig.1.17**. It can also be seen in **Fig. 1.17** that, typical ferroelectric oxides have a band gap more than 3 eV, except $BiFeO_3$, while SbSI has band gap about 2 eV but SbSI is not as strongly ferroelectric as the ABO_3 oxides. It has been investigated experimentally that substitution of cations like Ni, Fe and Mn-ions at Ti-site in $PbTiO_3$ reduced the band gap from 3.30 eV to 2.51 eV, 2.53 eV and 2.62 eV respectively as depicted in **Fig. 1.18** [15]. However, the crystal structure modifications also happen in such a way that

c/a ratio decreases in comparison to pure $PbTiO_3$ as can be seen in **Fig. 1.19**. This decrement in c/a ratio deteriorates the polarization. Another example for $PbTiO_3$ based material with very high-voltage photovoltaic effect is reported by K. Uchino. et. al. in $0.895PbTiO_3$-$0.105La(Zn_{2/3}Nb_{1/3})O_3$ ceramics [79].

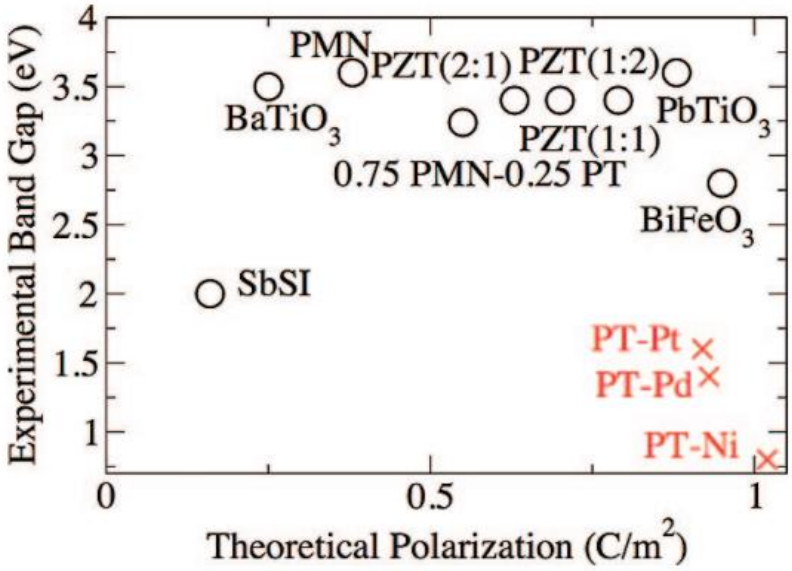

Figure 1.17: Illustration of band gap variation of ferroelectrics materials obtained experimentally with their theoretical polarization [72].

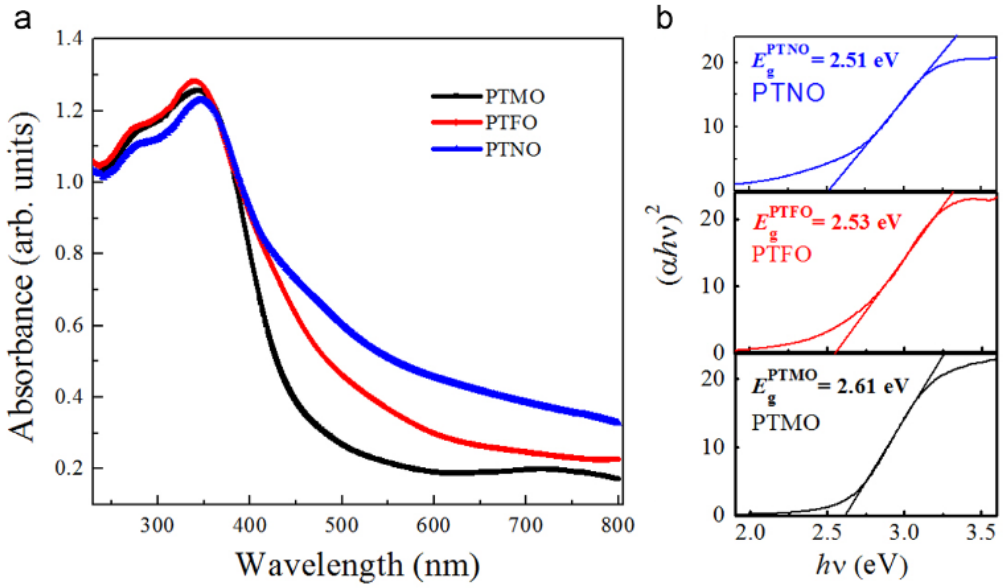

Figure 1.18: (a) Absorption curve and (b) band gap for $PbTi_{0.95}TM_{0.05}O_3$ TM = Mn, Fe and Ni [15].

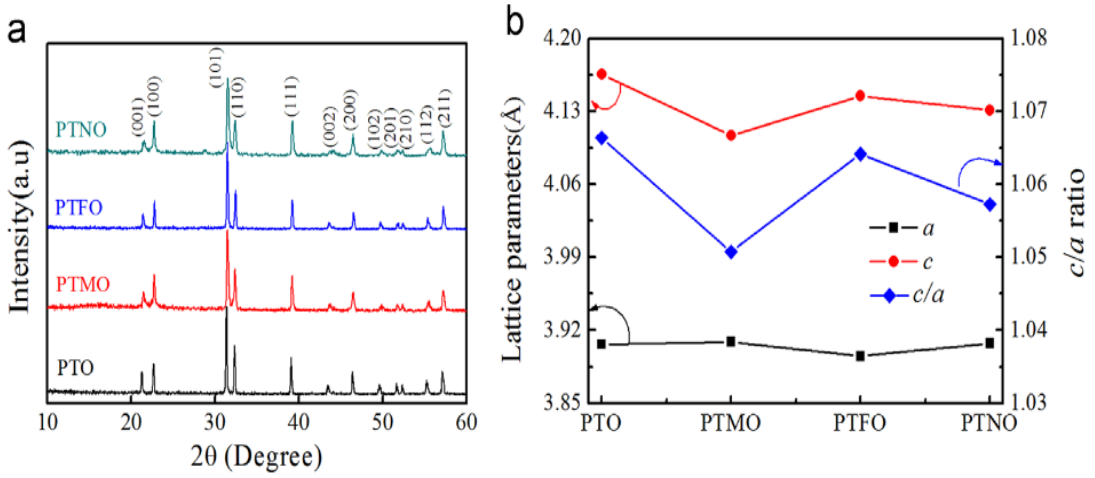

Figure 1.19: (a) Crystal structure and (b) tetragonality for $PbTi_{0.95}TM_{0.05}O_3$, TM = Mn, Fe and Ni [15].

Theoretically Ni doped PTO shows very low band gap ~ 0.8 eV whereas G. Y. Gou et. al. reported the experimental band gap value to be 2.42 eV [80]. In Ni doped PTO, Ni-3d states are lower in energy than the conduction band, localized around Ti-3d orbital of pure PTO and fall near conduction band in the band gap, thereby extend the conduction band towards lower energy. Thus reduction in band gap is observed for doping of transition element in $PbTiO_3$ [72]. In case of $PbTi_{1-x}Ni_xO_3$ thin film, the band gap was reported to be 2.86 eV and good remnant polarization of 58.1 $\mu C/cm^2$ was obtained. The Ni doped PTO films show better photocurrent as compared to pure PTO films [81]. Almost similar mechanism is observed for doping of various transition metal in $PbTiO_3$.

Conclusively in $PbTiO_3$, unfilled d-orbitals of Ti^{4+} favour ferroelectricity by forming a stable hybridized bond with the apical O^{2-} ions. Therefore, replacing Ti by another metal having partially filled d-orbital is undesirable for retaining ferroelectric behaviour. However, $PbTiO_3$ can be chosen as the base material for doping because it shows high polarization and small substitution at the Ti-site is not going to deteriorate much the polarization. Many successful attempts are reported in this direction showing the significant reduction in band gap.

1.7.2 Bismuth Ferrite ($BiFeO_3$) based ceramics

$BiFeO_3$ (BFO) is the most investigated material in the field of ferroelectric photovoltaic applications. It is one of the most attractive multiferroic material due to presence of large spontaneous polarization (~ 100μC/cm^2) at room temperature and very high Curie temperature (~1100K), much higher than $PbTiO_3$ (~753K) and $BaTiO_3$ (~400 K) [63, 82]. BFO has ABO_3 type perovskite crystal structure and has been investigated in single crystal and epitaxial thin film form in many device applications. Synthesis of single phase stoichiometric $BiFeO_3$ is difficult due to the excess Bi-loss during sintering and existence of secondary phases. Even if anyhow single phase is prepared, the leakage current due to oxygen vacancies is so high that it is difficult to pole the sample and measure the hysteresis loop. To overcome this problem, chemical modifications are performed in the expectation for facile preparation which can also alter or improve the physical properties of $BiFeO_3$. Various cationic doping on either Bi-site or on Fe-site or on both the sites are reported in literature [83]. **Table 1.1** lists the polarization of $BiFeO_3$ and Bi-site substituted BFO ceramics whereas **Table 1.2** lists the Fe-site substituted BFO ceramics [83]. General observation of both the tables reveals that substitution at Bi-site enhances the polarization in many cases while substitution at Fe-site have tendency to reduce the polarization. Sm-doping on Bi-site, Nd-Mn co-doping on Bi-Fe sites have promptly enhanced the polarization upto 50 μC/cm^2 from 10 μC/cm^2 of pure $BiFeO_3$ ceramics. Yb-substitution on Bi-site reduces the band gap to 2.03 eV which absorb considerable amount of spectra in visible region, as shown in **Fig.1.20** [84]. Thus, as a concluding remark, we can say that the band gap of BFO is tuneable in a wide range (1.5 eV – 2.1 eV) of band gap depending on the alloying elements and preparation method.

Table 1.1: Structure and physical properties of Bi-site doped $BiFeO_3$ ceramics [83].

Material system	Phase structure	d_{33} (pC/N)	P_r (μC/cm^2)	E_C (kV/cm)	M_r (emu/g)
$BiFeO_3$	R	27	~10	~70	–
$Bi_{0.88}Sm_{0.12}FeO_3$ (x = 0.05)	R	–	40~50	130	
$Bi_{0.875}Sm_{0.125}FeO_3$	Triclinic	29	15.1	90	0.071
$Bi_{1-x}Sm_xFeO_3$ (x = 0.125)	R	45	40	150	–
$Bi_{0.95}Dy_{0.05}FeO_3$	–	–	31	120	0.021
$Bi_{1-x}Dy_xFeO_3$	R~R-O	12–40 ($x \geqslant 0.08$)	6.1–15 (x = 0.10)	60–110	
$Bi_{1-x}Nd_xFeO_3$	R-triclinic-pseudo-T	–	9–1.9	–	0–0.23
$Bi_{1-x}Nd_xFeO_3$	R	28	–	–	–
$Bi_{1-x}La_xFeO_3$	R-triclinic-pseudo-T	>25	9.8	–	0.20
$Bi_{0.9}La_{0.1}FeO_3$	R	–	~6.0	–	–
$Bi_{0.85}La_{0.15}FeO_3$	Pseudocubic + triclinic	27.7	12	60	0.0744
$Bi_{1-x}Ce_xFeO_3$ (x = 0.15)	R	–	8.4	70	–
$Bi_{0.95}Ho_{0.05}FeO_3$	–	–	1.59	5.45	0.736
$Bi_{0.9}Ho_{0.1}FeO_3$	R	–	12.5	63	0.028
$Bi_{1-x}Yb_xFeO_3$ (x = 0.15)	R	–	8.5	~50	–
$Bi_{1-x}Eu_xFeO_3$ (x = 0.10)	R~R-O	–	–	–	0.075
(Eu,Gd,Tb,Dy)-$BiFeO_3$	R	48–49	21–35	106–117	0.016–0.044
$Bi_{1-x}Pr_xFeO_3$ (x = 0.20)	R	–	–	–	0.0051
$Bi_{1-x}Sr_xFeO_3$ (x = 0.3)	Triclinic	–	–	–	0.09
$Bi_{0.74}Ba_{0.30}FeO_3$	Pseudo-tetragonal	–	–	–	0.16
$Bi_{1-x}Ba_xFeO_3$	–	–	~5.5	–	~0.75
$Bi_{1-x}Ca_xFeO_3$	R-triclinic	–	–	–	~0.034
$Bi_{1-x-y}Sm_xLa_yFeO_3$	Triclinic	50	1.38	58.5	–

Table 1.2: Structure and physical properties of Fe-site doped $BiFeO_3$ ceramics [83].

Material system	Phase structure	P_r (μC/cm^2)	E_C (kV/cm)	M_r (emu/g)
$BiFe_{0.75}Ti_{0.25}O_3$	–	0.081	2.571	0.025
$BiFe_{0.95}Co_{0.05}O_3$	R	–	–	0.7
$BiFe_{0.95}Zn_{0.05}O_3$	–	–	–	–
$BiFe_{1-x}Mn_xO_3$	R	3.99	19.79	–
$BiFe_{1-x}Ti_xO_3$	R~R-O	–	–	–
$BiFe_{1-x}Sc_xO_3$	R	–	–	0.24–1.7 m
$BiFe_{1-x}Ta_xO_{3+x}$	–	0.22	–	0.06
$BiFe_{1-x}Nb_xO_3$	–	–	–	0.015
$BiFe_{1-x}Nb_xO_3$	R	–	–	–
$BiFe_{1-x}Ho_xO_3$ (x = 0.05)	R	8.4	~75	0.0258
$BiFe_{0.95}Ni_{0.05}O_3$	R	–	–	0.1

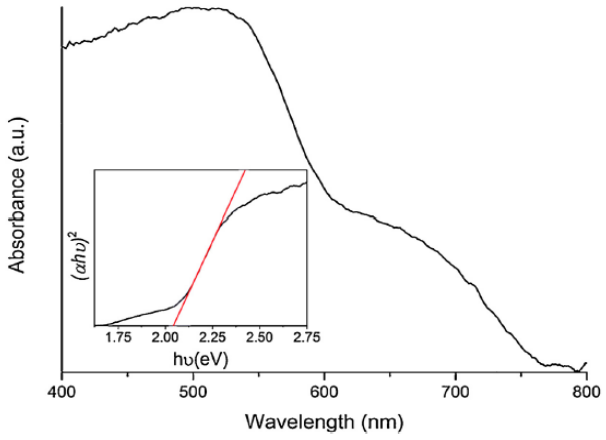

Figure 1.20: UV-vis diffuse reflectance spectra and the band gap of the $Bi_{1-x}Yb_xFeO_3$ sample with x = 0.05 [84].

Fig. 1.21 shows the plot of absorption curve with energy and inset shows band gap versus temperature variation with vertical lines showing the transition temperature for BFO thin film. Transition metal ions with partially filled d-orbitals in BFO are reported to be responsible for relatively low band gap as compared to other ABO_3 ferroelectric oxides [85]. Many research groups have prepared epitaxial thin films of BFO successfully and observed substantial photovoltaic effect [82, 86]. Photoconductivity in multiferroic BFO thin film depends on incident light polarization, ferroelectric polarization of the material and crystallographic symmetry [86]. S. R. Basu et. al. have obtained good photoconductivity in BFO thin film but low V_{oc} [82]. S. Y. Yang et al have reported variation of V_{oc} with changing orientation of electrode and claimed very high above band gap voltage (V_{oc} ~16 kV/cm) in epitaxial BFO film when Pt electrodes were perpendicular to domain walls (71° array). However, good photoconductivity but no V_{oc} was observed when Pt electrode was parallel to domain walls. Physical origin of this phenomena in ferroelectric materials is explained by domain wall theory.

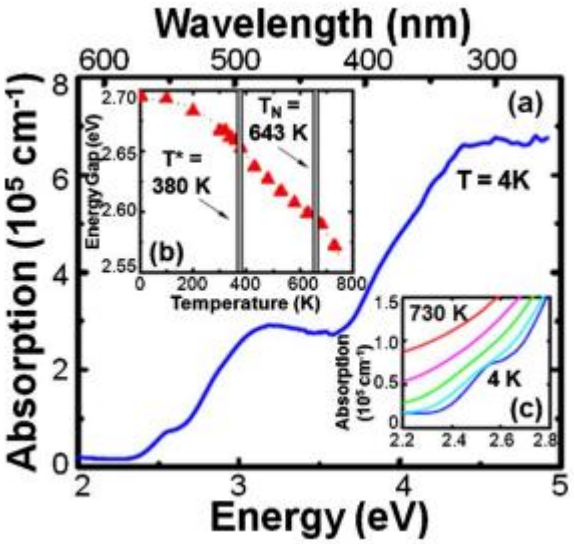

Figure 1.21:. (a) Optical absorption of a 100 nm thick BFO film prepared on $DyScO_3$ substrate at 4 K. (b) Band gap variation as a function of temperature (c) Zoomed view of the shoulder at 2.5 eV [82].

1.7.2.1 $KBiFe_2O_5$ Ceramics

G. Zhang et. al. report a novel Bi based ferroelectric compound $KBiFe_2O_5$ which has MO_4 tetrahedral network with orthorhombic crystal structure, narrow band gap of 1.6 eV, higher conductivity and high Curie Temperature (T_c -780K). The material belongs to $A_2B_2O_5$ family and has properties suitable for solar energy applications. This is evidenced that ferroelectrics with metal oxygen tetrahedral network (MO_4) have smaller band gap than the traditional common ferroelectrics with MO_6 octahedral network. Fig. 1.22 shows that all the wavelengths up to 750 nm are absorbed by $KBiFe_2O_5$ with good absorption coefficient (10^4 cm^{-1}) utilising the visible region along with the UV region of solar spectra. As can be seen in **Fig. 1.22** and **Fig. 1.23**, the band gap (1.6 eV) of $KBiFe_2O_5$ is near ideal value which can achieve theoretically maximum efficiency about 30%. It is notable that due to low band gap high leakage is possible which complicate the data interpretation of polarization. The leakage is observed to be high in the ceramic samples than single crystals. Fig. 1.24 shows the hysteresis loop of single crystal $KBiFe_2O_5$ validating the weak ferroelectric nature. The loop is unsaturated because breakdown happens due to high leakage. Current-voltage (I-V) characteristic of the sample measured under illumination of a UV-light (4 mW/cm^2) clearly shows significant photovoltaic behaviour with V_{oc} = 9.1 eV and photocurrent density 15 $\mu A/cm^2$ suggesting the polar nature of the material. Presence of open circuit voltage larger than the band gap (E_g) is a characteristic property of photovoltaic effect in ferroelectric materials. This above band gap open circuit voltage provides a platform where more durable and more efficient materials can be evolved for solar energy harvesting applications.

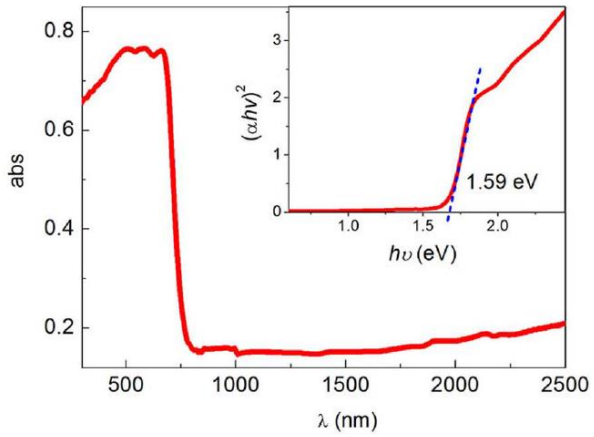

Figure 1.22: UV-Vis-near IR absorption spectrum of $KBiFe_2O_5$ [68].

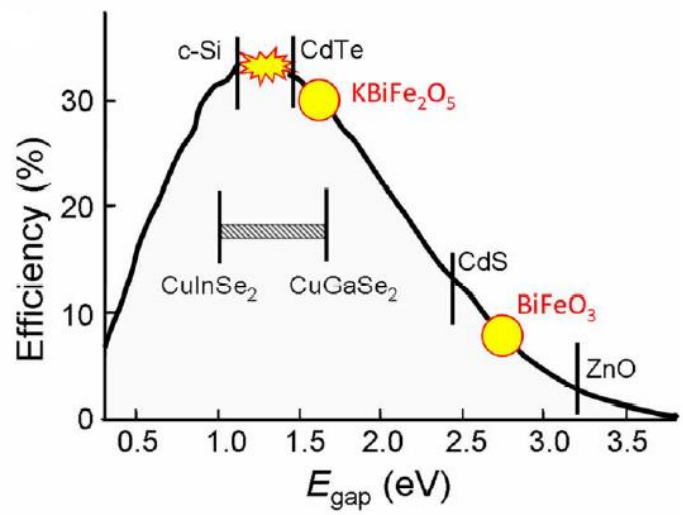

Figure 1.23: Variation of maximum theoretical efficiency obtained at a band gap for AM1.5 illumination [68].

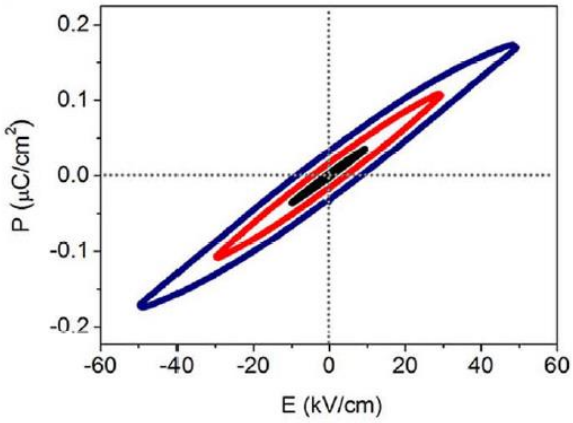

Figure 1.24: P-E hysteresis loops of single crystal $KBiFe_2O_5$ measured at room temperature [68].

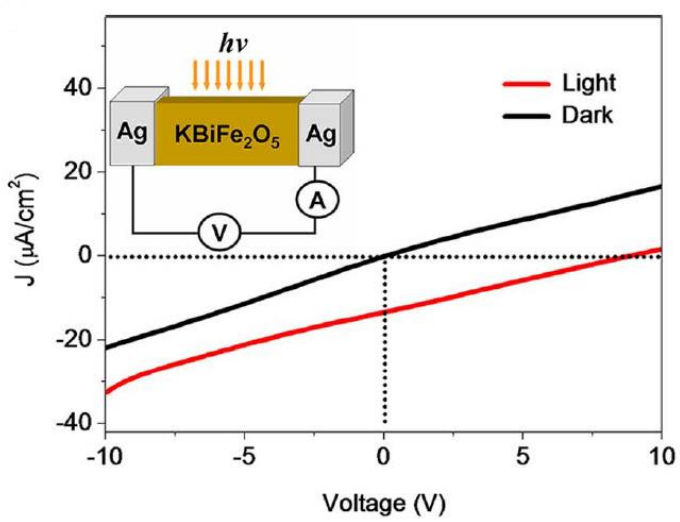

Figure 1.25: Current density curve in the dark and UV illumination [68].

1.7.2.2 Bi_2FeCrO_6 Ceramics

Many double perovskites e. g. Bi_2FeCrO_6, Bi_2NiMnO_6, Bi_2FeMnO_6 have been investigated for their unique multiferroic properties [87-89]. Multiferroic materials show ferroelectric property even with the partially filled d-orbitals which have better tendency (than typical ferroelectrics) to possess low band gap suitable for photovoltaic applications. Heng Wu et. al. studied the physical properties of Bi_2FeCrO_6 ceramics and found that it has significantly low band gap ~1.5 eV which can effectively absorb the large portion of sunlight, as illustrated in **Fig. 1.26** [90]. L. Sha et. al. studied the ferroelectric properties of the BFO and BFCO thin films as shown in **Fig. 1.27**. Presence of switchable ferroelectric polarization were observed in both the polycrystalline films, and BFCO film ($2P_r$ = 19.8 μC/cm^2) shows better remanent polarization than BFO film ($2P_r$ = 8.7 μC/cm^2). It was difficult to achieve the saturation in polarization for both the BFO and BFCO thin films due to high leakage current but, leakage in BFCO thin film was reported to be lesser than the BFO film [87].

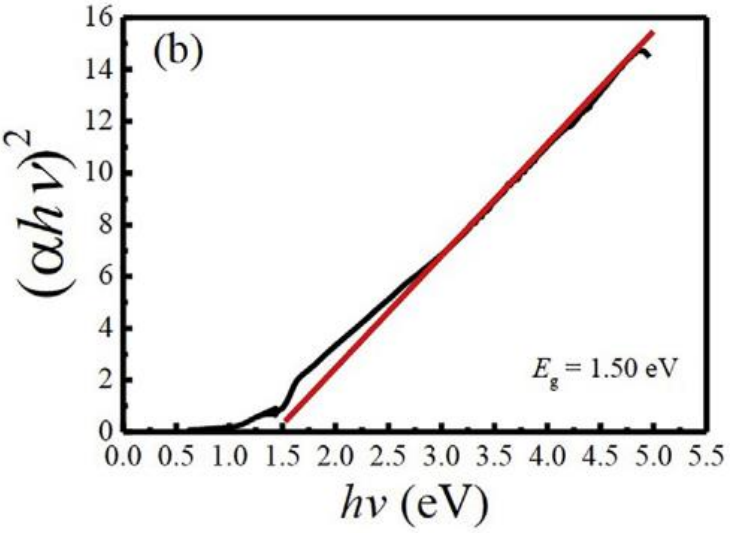

Figure 1.26: Band gap energy of double perovskite Bi_2FeCrO_6 [90].

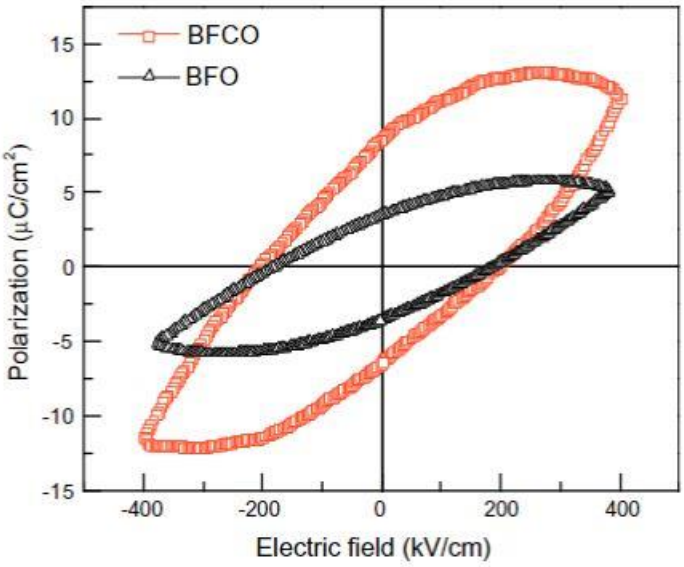

Figure 1.27: A comparison of hysteresis loops of thin film of Bi_2FeCrO_6 with $BiFeO_3$ [87].

R. Nechache et. al. prepared multilayer BFCO thin film and obtained excellent power conversion efficiency about 8% under AM 1.5 G irradiation (100 mW cm^{-2}) [23]. The authors showed that the band gap of thin films depend on deposition rate and epitaxial strain present in it. They fabricated two multilayer structures at different temperatures M1 (1.6 eV) at 580°C and M2 (1.3 eV) at 720°C composed of three BFCO

consecutive layer (S1, S2 and S3) deposited on Nb-doped $SrTiO_3$ at different deposition rate. The deposition rate for individual layers was chosen in such a way that largest band gap layer lies on top and rear most layer have the least band gap. Superposition of the absorption coefficients of this multilayer structure allows broad absorption, covering the complete area of visible and UV region of solar spectrum. The power conversion efficiency of individual layer and multilayer is shown in Table 1.3. Multilayer M1 (1.6 eV) has much better polarization (35 $\mu C/cm^2$) than multilayer M2 (15 $\mu C/cm^2$). Hence optimized layer M1 shows the unprecedented efficiency of 8.1 % showing enormous potential as active layer for efficient PV devices.

Table 1.3: Performance of single layer and multilayer Bi_2FeCrO_6 devices [23].

	J_{sc} (mA cm^{-2})	V_{oc} (V)	FF (%)	PCE (%)
S1	11.7	0.79	36	3.3
S2	10.8	0.65	29	2.1
S3	2.8	0.66	27	0.5
M1	20.6	0.84	47	8.1
M2	23.6	0.56	33	4.3

1.7.3 Barium Titanate ($BaTiO_3$) Based Ceramics

Barium titanate (BT) is most preferred lead-free perovskite base material for energy storage and harvesting applications in ceramic devices. Photovoltaic effect in $BaTiO_3$ were first discovered way back in 1956. Phenomena of bulk photovoltaic effect in $BaTiO_3$ produces photovoltage (5V) above than the band gap (3.3 eV) [91]. It has high dielectric constant, high quality factor, low dielectric loss and good electromechanical coupling (k_{33}~50) making it suitable for multiverse functional applications. However, high band gap of pure $BaTiO_3$ (3.3 eV) restricts it use for photovoltaic applications and high hysteresis loss remains as major obstacle in energy storage applications. The wide band gap of this material, like in other perovskites, can be owed to d^0 configuration of the B-site transition metal (Ti^{4+}) anion. On the other hand, d^0 ness of B-site transition metal cation directly introduces the ferroelectricity.

Thus, attempts to reduce the band gap by substituting the d^0 ion by non- d^0 transition metal ions tends to deteriorate and destroy the ferroelectricity. Many substitutional replacements for Ti-ion in $BaTiO_3$ such as Cr^{3+}, Fe^{3+}/Fe^{2+}, Mn^{3+}, Co^{3+} and Ni^{2+} are reported to get accommodated easily [92-95]. In all these cases, band gap is lowered than that of pure $BaTiO_3$, facilitated by the charge transfer process via the mid gap defect states.

Substitution by Ni and Ni-Nb accompanied with some vacancies significantly reduced the band gap to ~1.5 eV [96]. Doping of double perovskite Sr_2KMoO_6 (K = Fe, Co, Ni, Mn) in $BaTiO_3$ reduces the band gap from 3.22 eV to 1.77 eV subsequently. [97]. Xiao et. al. reported sufficiently lower band gap in $0.95Na_{0.5}Bi_{0.5}TiO_3$-$0.05BaTiO_3$ solid solution after introducing Ni^{2+} at the Ti-site. It shows three absorption edges with lowest sub band gap of ~1 eV [45]. D. Das et. al. have reported a breakthrough result by co-doping a John-Teller Cation Mn^{3+} and Nb^{5+} for two Ti sites in $BaTiO_3$. This approach not only reduced the band gap from 3.18 eV to 1.66 eV but also retained appreciable polarization value (70% of $BaTiO_3$) at room temperature [22]. A Zenkevich et. al. reported the photovoltaic effect in $BaTiO_3$ thin film prepared on MgO substrate by pulse laser deposition method. **Fig. 1.28** shows the schematic diagram for the structure and photovoltaic investigation of the thin film on MgO substrate. Linear J-V curves (continuous line) under the illumination of UV light are extrapolated to V-axis (voltage) to obtain the open circuit photo voltage (V_{oc}) [98]. The photovoltage obtained was 0.65V for 50 nm thin film and the corresponding photo induced electric field was E_{pv} = $1.3x10^5$ V/cm, as shown in **Fig. 1.29**. The energy conversion efficiency η due to bulk photovoltaic effect was about~ 1% which is still very much low than commercially available photovoltaic solar cells.

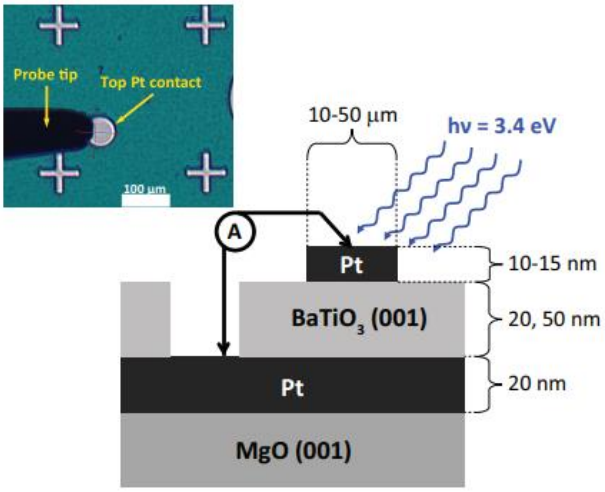

Figure 1.28: Bulk photovoltaic effect in $BaTiO_3$ thin film made on MgO substrate (Inset: microscopic view of the sample [98].

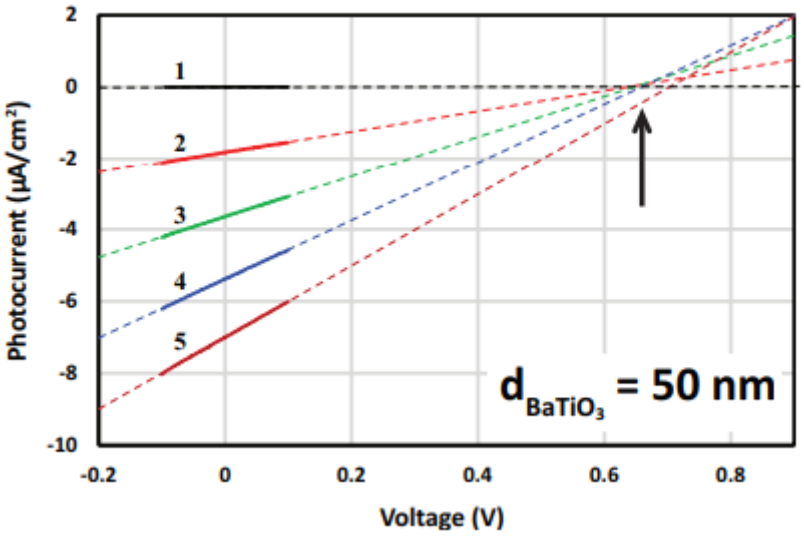

Figure 1.29: J-V characteristics for $Pt/BaTiO_3/Pt$ thin film on MgO substrate under different illumination. (1: dark current, 2: I = 1.5 x 10^{-1}, 3: I = 3 x 10^{-1}, 4: I = 4.5 x 10^{-1},5: I = 7.5 x 10^{-1}) [98].

1.7.3.1 Mn-Nb co-doped $BaTiO_3$

Das et. al. has adopted a strategy to co-dope a pair of John Teller cations Mn^{3+} and Nb^{5+} for a pair of Ti at B-site in $BaTiO_3$ and obtained very low band gap (1.66 eV) with sizable polarization. The results of Mn-Nb co-doping were also compared with the results of Fe-Nb co-doping where Mn^{3+} is replaced by a non-John Teller cation Fe^{3+}. In this strategy, Mn^{3+} having non-d^0 configuration (d^4) is chosen to reduce the band gap

and Nb^{5+} is selected to retain the ferroelectricity. Transition metal cation Mn^{3+} is acceptor ion and Nb^{5+} is donor ion forming a charge neutral configuration, however the pair have a finite electric dipole which tends to enhance the polarization. **Fig. 1.30(a)** shows the comparative structural changes evolving with increasing concentration of Mn and Fe and **Fig. 1.30 (b)** illustrates the splitting of (200) planes XRD peak. It is evident that the tetragonal distortion decreases with the replacement of Ti, in both the cases. The figure further illustrates that the (200) peak splitting corresponding to the tetragonal structure, is much smaller in the case of Fe-Nb co-doping than the Mn-Nb co-doping. This imply that ferroelectric property decreases much faster for substitution of non-John-Teller cation than that of John-Teller cation. Among all, $BaTi_{1-x}(Mn_{1/2}Nb_{1/2})_xO_3$ with composition x = 0.15 was found to have lowest band gap (1.3 eV), as shown in **Fig 1.31,** but, on the other, hand polarization vanishes for this level of doping.

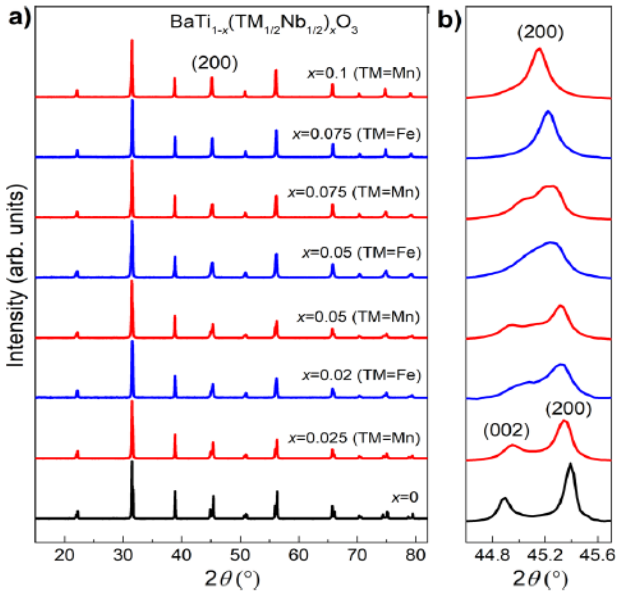

Figure 1.30 : (a) Structural evolution of $BaTi_{1-x}(Mn_{1/2}Nb_{1/2})_xO_3$ series (in red lines) and of $BaTi_{1-x}(Fe_{1/2}Nb_{1/2})_xO_3$ series (in blue line) (b) Magnified (200) and (002) peak showing tetragonal distortion with Ti-substitution [22].

The composition with x = 0.075 is the optimum combination of low band gap (1.6 eV) and significant polarization (15.4 $\mu C/cm^2$) at room temperature. Comparison with the

best results for ferroelectric photovoltaic materials reported in literature shows that Mn-Nb co-doped BTO samples have performed quite well.

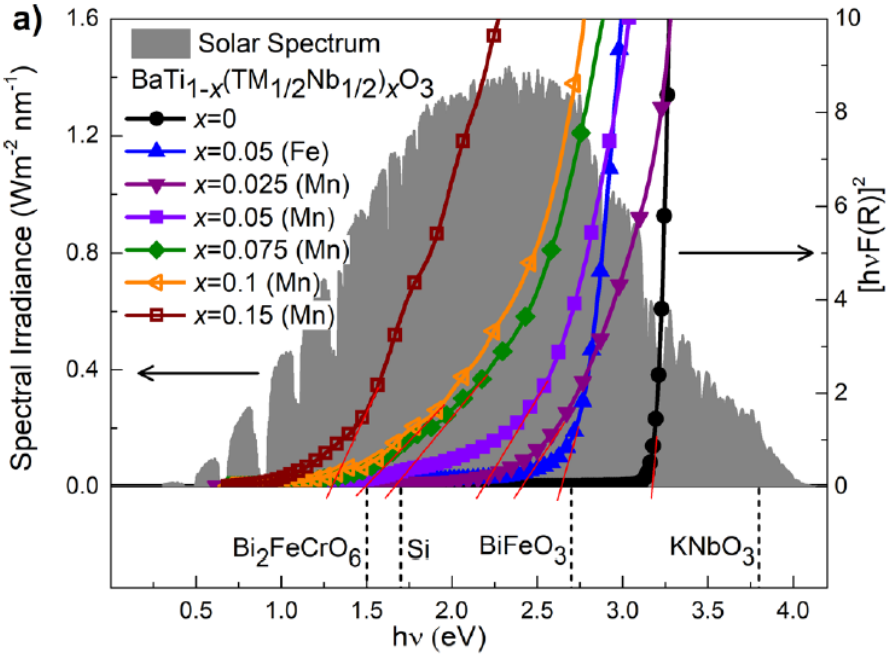

Figure 1.31: Band gap of various compositions of $BaTi_{1-x}(Mn_{1/2}Nb_{1/2})_xO_3$ compared with Mn replaced by Fe and some other potential photo-ferroelectric materials [22].

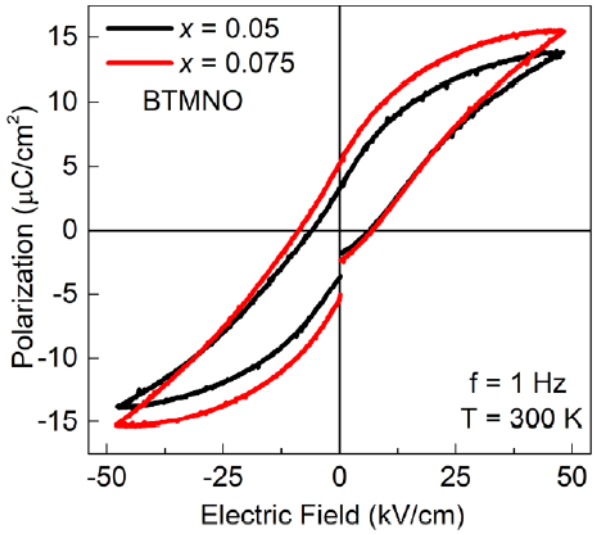

Figure 1.32: Significant room temperature polarization of $BaTi_{1-x}(Mn_{1/2}Nb_{1/2})_xO_3$ with x = 0.50 and 0.75 [22].

1.7.4 Other Attractive Materials

1.7.4.1 $(KNbO_3)_{1-x}(BaNi_{1/2}Nb_{1/2}O_3)_x$ (KNO-BNNO) Solid Solution

I. Grinberg et. al. also used the strategy of doping two different transition metal cation on the B-site to obtain a photo- ferroelectric material, one chosen to retain ferroelectricity and other to bring the band gap in visible range. A classic ferroelectric material $KNbO_3$ were chosen as parent material which have off-centred distortion and high polarization (50 $\mu C/cm^2$). Moreover, Nb containing materials have tendency to tolerate high concentration of vacancies. The authors developed a thin film of $(KNbO_3)_{1-x}(BaNi_{1/2}Nb_{1/2}O_3)_x$ (KN-BNNO), where Ni- and Nb- were introduced at the B-site, showing wide band gap tunability of band gap from 1.18 eV to 3.8 eV [29]. Wide range variation of band gap, as shown in **Fig. 1.33**, can utilise most of the solar spectrum. Specially the composition with x = 0.10 has the direct band gap of 1.39 eV with polar property at room temperature and much higher photocurrent density (50 times) than typical piezoelectric PZT.

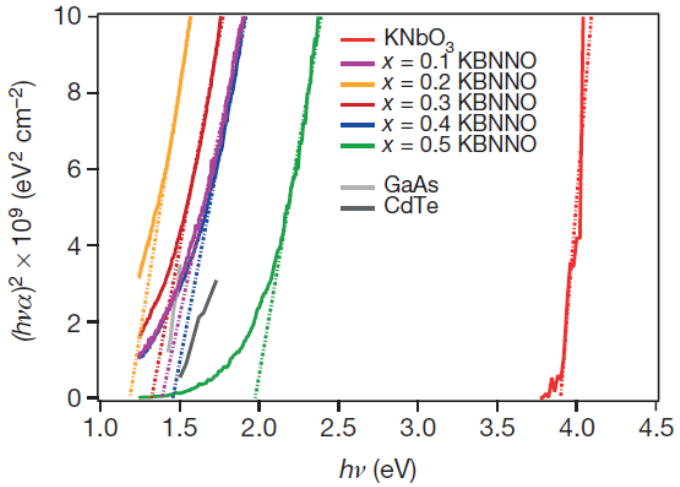

Figure 1.33: Determination of band gap for KBNNO oxides with x = 0.1–0.5 [29].

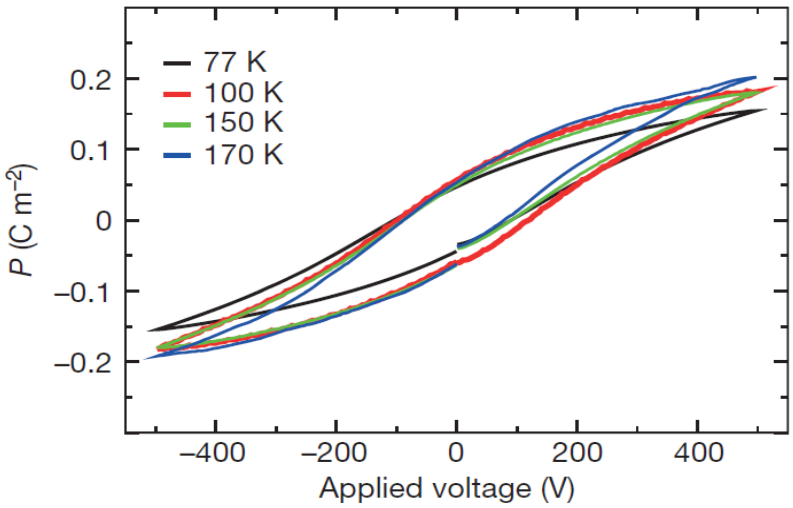

Fig. 1.34 Ferroelectric hysteresis loops for a 20-microm-thick x =0.1 KBNNO film at 77–170 K [29].

Significantly lower band gap (1.39 eV) for KN-BNNO (with x = 0.10) than the parent material (3.8 eV) was observed suitable to utilise the complete visible region (< 1.65 eV) as well as the infrared region. However, BNNO substitution decreased the polarization, even though it is smaller than the parent material but still substantial. The photo response measured at 77K sample poled at 500V pulse were observed much better than the response in classical ferroelectrics like (Pb,La)(Zr,Ti)O_3 and (Na,K)NbO_3 [19, 99, 100]. Open-circuit photovoltage (V_{oc}) and short-circuit photocurrent (J_{sc}) were found to be 3.5 V and 40 nA cm^{-2} adding to the previous reports of above band gap voltage.

1.7.4.2 List of ferro-photovoltaic materials investigated in recent years

Rigorous research on photo-ferroelectric materials is bringing novel materials every year with new strategies. A comparison for band gap and the polarization values of some of the potential materials, reported in past is listed in the **Table 1.4** below:

Table 1.4: List of the experimental band gap of various pure and doped ferroelectric materials.

Material name	Material's Form	Band Gap (eV)	Maximum Polarization (reported) ($\mu C/cm^2$)	Reference
$BiFeO_3$	Single crystal and thin film	2.7	60	[82]
$BiFe_{1-x}Mn_xO_3$	Thin Film	1.1	-	[101]
$Bi_{1-x}Yb_xFeO_3$	Powder Ceramics	2.03	-	[84]
$KBiFe_2O_5$	Single Crystal	1.6	3.73	[68]
Bi_2FeCrO_6	Thin Film	1.4	50-90	[102]
$YbFeO_3$	Nano Crystalline	2	4	[103]
$PbTiO_3$ Ni-doped $PbTiO_3$ Fe-doped $PbTiO_3$ Mn-doped $PbTiO_3$	Powder Ceramics	3.2 2.51 2.53 2.61	- - - -	[15]
$PbTiO_3$-$Bi(Co_{2/3}Nb_{1/3})O_3$	Powder Ceramics	2.2 - 2.6	-	[38]
$PbTiO_3$-$Bi(Ni_{2/3}Ta_{1/3})O_3$	Powder Ceramics	2.25-1.85	35-40	[20]
$BaTiO_3$	Single Crystal thin film	3.3	25	[104]
$BaTi_{0.925}(Mn_{1/2}Nb_{1/2})_{0.075}O_3$	Bulk Crystal	1.66	15	[22]
$LiNbO_3$	Single crystal	3.78	71	[105, 106]
(1-x)$KNbO_3$-x$Ba(Ni_{1/2}Nb_{1/2})O_{3-\delta}$	Bulk Crystal	1.1 -3.8	0-5	[29]
$(K_{0.9}Ba_{0.1})(Nb_{0.95}Ni_{0.05})O_{3-0.025}$	Powder Ceramics	1.40	8	[107]

1.8 $BaTiO_3$ based ferroelectric materials having energy storage properties

Analysis of the various materials used for photovoltaic energy harvesting and energy storage applications infers that relaxor ferroelectric materials are the class of materials which is used in both kind of applications. It is shown in previous sections that many $BaTiO_3$ based materials have potential for photovoltaic applications after proper modification. Many $BaTiO_3$ based ferroelectric materials are also useful in

energy storage applications. $BaTiO_3$ shows very high polarization but unfortunately, high hysteresis loss has restricted the energy storage efficiency below 80%. In order to achieve very high recoverable energy density (W_{rec}) and high efficiency (η) simultaneously, narrow and oblique shaped P-E loops need to be obtained [108]. In this context, relaxor ferroelectrics which have constricted P-E loop, and high electric breakdown strength appears to be most interesting among all ferroelectrics [109, 110]. Many $BaTiO_3$ based relaxor ferroelectrics have also shown relatively low band gap [111, 112]. Conclusively, suitable chemical modification of the $BaTiO_3$ may provide a versatile material useful in energy harvesting and storage applications.

1.9 Objective of present work

On the basis of the literature discussed in preceding sections, it can be inferred that band gap engineering by transition metal cation doping is the facile and effective way to find the suitable material for photovoltaic application. Our motive is to investigate the selection of the suitable dopants and base materials to get optimal band gap and ferroelectricity in the developed materials. To meet these goals, the important objectives undertaken in the thesis are following:

1. To modify the typical ferroelectric material $PbTiO_3$ by doping of Mo ion suitable for FEPV application and to study the effect of doping on structural, morphological, absorption, dielectric and ferroelectric properties of the developed material.
2. To develop a novel Bi-based solid solution ($BiMnO_3$-$BiYO_3$) suitable for FEPV application and to examine the structural, morphological, absorption, dielectric and ferroelectric properties of the various compositions.

3. To develop a $BaTiO_3$ based, lead-free photo-ferroelectric material by co-doping of cheaper elements, Bi and Li and to investigate the effects of co-doping on the physical properties of the materials